Chinese Journal of Natural Medicines

***Platycodon grandiflorus* polysaccharides combined with hesperidin exerted the synergistic effect of relieving ulcerative colitis in mice by modulating PI3K/AKT and JAK2/STAT3 signaling pathways**

Yang Liu, Quanwei Sun, Xuefei Xu, Mengmeng Li, Wenheng Gao, Yunlong Li, Ye Yang, Dengke Yin

Citation: Yang Liu, Quanwei Sun, Xuefei Xu, Mengmeng Li, Wenheng Gao, Yunlong Li, Ye Yang, Dengke Yin, *Platycodon grandiflorus* polysaccharides combined with hesperidin exerted the synergistic effect of relieving ulcerative colitis in mice by modulating PI3K/AKT and JAK2/STAT3 signaling pathways, Chinese Journal of Natural Medicines, 2025, 23(7), 848−862. doi: 10.1016/S1875−5364(25)60913−7.

View online: https://doi.org/10.1016/S1875−5364(25)60913−7

Chinese Journal of Natural Medicines 23 (2025) 848-862

Contents lists available at ScienceDirect

Chinese Journal of Natural Medicines

journal homepage: www.cjnmcpu.com/

Original article

Platycodon grandiflorus polysaccharides combined with hesperidin exerted the synergistic effect of relieving ulcerative colitis in mice by modulating PI3K/AKT and JAK2/STAT3 signaling pathways

Yang Liu[a], Quanwei Sun[a], Xuefei Xu[b], Mengmeng Li[a], Wenheng Gao[a], Yunlong Li[a], Ye Yang[a,c,*], Dengke Yin[a,c,d,e,*]

[a] *School of Pharmacy, Anhui University of Chinese Medicine, Hefei 230012, China*
[b] *School of Basic Medical Sciences, Zhejiang Chinese Medical University, Hangzhou 310053, China*
[c] *Anhui Provincial Key Laboratory of Pharmaceutical Preparation Technology and Application, Anhui University of Chinese Medicine, Hefei 230021, China*
[d] *Anhui Provincial Key Laboratory of Traditional Chinese Medicine Formula Granule, Anhui Huarun Jinchan Pharmaceutical Co., Ltd., Huaibei 235000, China*
[e] *Anhui Provincial Key Laboratory of Research & Development of Chinese Medicine, Anhui University of Chinese Medicine, Hefei 230021, China*

ARTICLE INFO

Article history:
Received 26 February 2024
Revised 21 April 2024
Accepted 7 July 2024
Available online 20 July 2025

Keywords:
Ulcerative colitis
Platycodon grandiflorus polysaccharides
Hesperidin
Synergistic effects
PI3K/AKT
JAK2/STAT3

ABSTRACT

Ulcerative colitis (UC) is a chronic inflammatory disorder with a complex etiology, characterized by intestinal inflammation and barrier dysfunction. *Platycodon grandiflorus* polysaccharides (PGP), the primary component of *Platycodon grandiflorus*, and hesperidin (Hesp), a prominent active component in *Citrus aurantium* L. (CAL), have both demonstrated anti-inflammatory properties. This study aims to elucidate the underlying mechanism of the synergistic effect of PGP combined with Hesp on UC, focusing on the coordinated interaction between the phosphatidylinositol 3-kinase (PI3K)/protein kinase B (AKT) and Janus kinase 2 (JAK2)/signal transducer and activator of transcription 3 (STAT3) signaling pathways. A mouse model of UC induced by dextran sulfate sodium (DSS) and a cell model using lipopolysaccharide (LPS)-induced RAW264.7/IEC6 cells were employed to investigate the *in vitro* and *in vivo* anti-inflammatory effects of PGP combined with Hesp on UC and its potential mechanism of action. The results indicated that compared to the effects of either drug alone, the combination of PGP and Hesp significantly modulated inflammatory factor levels, inhibited oxidative stress, regulated colonic mucosal immunity, suppressed apoptosis, and restored intestinal barrier function *in vitro* and *in vivo*. Further *in vitro* studies revealed that PGP significantly inhibited the PI3K/AKT signaling pathway, while Hesp significantly inhibited the JAK2/STAT3 signaling pathway. The use of inhibitors and activators targeting both pathways validated the synergistic effects of PGP combined with Hesp on the PI3K/AKT and JAK2/STAT3 signaling pathways. These findings suggest that PGP combined with Hesp exhibits a synergistic effect on DSS-induced colitis, potentially mediated through the phosphatase and tensin homolog (PTEN)/PI3K/AKT and interleukin-6 (IL-6)/JAK2/STAT3 signaling pathways.

1. Introduction

Ulcerative colitis (UC) is a chronic, non-specific inflammatory bowel disease that affects the colonic mucosa, initiating in the rectal mucosa and extending proximally in a continuous manner throughout the colon [1, 2]. Recent reports indicate an increasing incidence and prevalence of UC, with an annual occurrence rate of 12.6 per 100 000 individuals in the UK [3, 4]. Accumulating evidence suggests that UC is a multifactorial disease arising from complex interactions between genetic, environmental, immune, and microbial factors, though the precise etiology remains elusive [5]. Currently, clinical management of UC primarily involves the administration of aminosalicylic acid, antibiotics, oral corticosteroids, and immunosuppressive agents. However, these treatments often present significant adverse effects and may lack efficacy across various stages of the disease [6]. Consequently, there is a pressing need to identify novel therapeutic approaches for the effective treatment of UC.

Current management of UC is primarily limited to monotherapy, and the potential advantages of combination therapy remain largely unexplored. Recent years have witnessed growing interest in utilizing bioactive natural compounds for UC treatment. Notably, polysaccharides and flavonoids, as effective dietary resources, have shown promising therapeutic potential in UC management, operating through various mechanisms [7]. *Platycodon grandiflorus* (PG), a traditional medicinal and edible plant, has been employed to treat various ailments due to its anti-inflammatory, antioxidant, immune-enhancing, and other biological properties [8]. The main component of polysaccharides is *Platycodon grandiflorus* polysaccharide (PGP). Previous research has demonstrated that PGP can exert significant therapeutic effects on UC in mice through anti-inflammatory and antioxidant path-

* Corresponding author.
E-mail addresses: Y.Yang@ahtcm.edu.cn (Y. Ye); yindengke@ahtcm.edu.cn (D. Yin)

https://doi.org/10.1016/S1875-5364(25)60913-7

ways [9, 10]. Further studies have revealed that PGP can inhibit the phosphatidylinositol 3-kinase (PI3K)/protein kinase B (AKT) signaling pathway. *Citrus aurantium* L. (CAL), a commonly consumed edible and medicinal resource in China, has extracts and major constituents reported to possess anti-cancer, antioxidant, anti-inflammatory, and vasodilatory properties [11]. Hesperidin (Hesp), one of the main active components in CAL, has been extensively studied for its ability to treat UC, with its mechanism involving the interleukin-6 (IL-6)/Janus kinase 2 (JAK2)/signal transducer and activator of transcription 3 (STAT3) pathway [12, 13].

Several studies have demonstrated that the JAK/STAT signaling pathway can interact with the PI3K/AKT signaling pathway *via* micro ribonucleic acid (miR)-21 and phosphatase and tensin homolog (PTEN) [14]. Additionally, research has shown that inhibiting STAT3 activation with JAK2 inhibitors suppresses the activation of nuclear factor κB (NF-κB) [15]. Based on the analysis of PGP and Hesp's action mechanism, we hypothesized that these compounds exert synergistic effects through PI3K/AKT and JAK2/STAT3 signaling pathways. To test this hypothesis, we established a mouse UC model and a RAW264.7/IEC6 cell inflammation model. These models were treated with PGP and Hesp, both individually and in combination, to elucidate their potential synergistic anti-inflammatory effects. By examining the impact of PGP and Hesp on the PI3K/AKT and JAK2/STAT3 pathways, our goal was to provide experimental evidence for the development of natural therapeutic agents like PGP and Hesp, offering potential new treatments for UC in clinical settings.

2. Materials and methods

2.1. Chemical reagent

The PG utilized in this study was obtained from Anhui Youxin Pharmaceutical Co., Ltd. (Anhui, China) and verified by Prof. Shoujin Liu of Anhui University of Chinese Medicine. PGP was prepared according to previously described methods [16]. Performance anion-exchange chromatography with pulsed amperometric detection was employed to analyze the polysaccharide composition of PGP. The analysis revealed that PGP comprised six polysaccharides: Fuc, Rha, Ara, Gal, Glc, and GalA, in a molar ratio of 11.00∶1.00∶15.79∶17.48∶12.45∶5.19, as illustrated in Supplement Fig. S1. FT-inhibition rate (IR) analysis results demonstrated that PGP exhibited characteristic absorption peaks of polysaccharides, as shown in Supplement Fig. S2. Hesp was sourced from Shanghai Yuanye Bio-Technology Co., Ltd. (Shanghai, China), while sulfasalazine enteric-coated tablets (SASP) was procured from Shanghai Xinyi Tianping Pharmaceutical Co., Ltd. (Shanghai, China). Dextran sulfate sodium (DSS) (MW: 36 000–50 000) was obtained from Dalian Meilun Biotech Co., Ltd. (Dalian, China). Malondialdehyde (MDA), T-SOD, and myeloperoxidase (MPO) kits were acquired from Nanjing Jiancheng Bioengineering Institute (Nanjing, China). Sparkzol reagent, cell counting kit-8 (CCK-8), colivelin, AG 490, and 740 Y-P were sourced from Shangdong Sparkjade Biotechnology Co., Ltd. (Jinan, China). LY294002 was obtained from Aladdin Biochemical Technology Co., Ltd. (Shanghai, China). Primary antibodies specific to ZO-1 were procured from Abcam (Cambridge, UK). Primary antibodies targeting β-actin, claudin-1, occludin, IL-6, PI3K, AKT, JAK2, STAT3, phosphorylated (p)-PI3K, p-AKT, p-JAK2, p-STAT3, and PTEN were purchased from Zen Bioscience Co., Ltd. (Chengdu, China). Primary antibodies specific to T helper type 2 (Th2) (IL-10) and regulatory T lymphocyte (Treg) [transforming growth factor β (TGF-β)], interferon γ (IFN-γ), IL-17, IL-10, IL-4, and IL-1β were acquired from Beijing Biosynthesis Biotechnology Co., Ltd. (Beijing, China). The primary antibody specific to tumor necrosis factor α (TNF-α) was supplied by Wanlei Biotechnology Co., Ltd. (Shenyang, China). Lipopolysaccharide (LPS) was purchased from Sigma Chemical Co., Ltd. (St. Louis, Missouri, USA). Enzyme-linked immunosorbent assay (ELISA) kits for detecting Mouse/Rat TNF-α, IL-1β, and IL-6 were obtained from Ruixin Biotechnology Co., Ltd. (Quanzhou, China). All other chemicals and solvents of analytical grade were sourced from Sinopharm Chemical Reagent Co., Ltd. (Shanghai, China).

2.2. Experimental animals and design

Male Balb/c mice (6–8 weeks old, weighing 20 ± 2 g) were obtained from Biotechnology Co., Ltd. (certificate number SCXK 2020-0009, Jiangsu, China) and housed in a controlled environment with a 12-h light/dark cycle. The mice were provided with a standard laboratory diet and water ad libitum. All animal experiments and procedures were reviewed and approved by the Institutional Ethics Committee of the Anhui University of Chinese Medicine (Ethical number: AHUCM-mouse-2021028). The experiments were conducted in accordance with the approved guidelines.

The study comprised six groups of mice (n = 6 per group): control group (CTL), model group (DSS), SASP group (200 mg·kg^{-1}), PGP group (400 mg·kg^{-1}), Hesp group (80 mg·kg^{-1}), and PGP + Hesp group (400 mg·kg^{-1} + 80 mg·kg^{-1}). The CTL group received normal drinking water, while the other five groups were given freshly prepared 3% DSS solution ad libitum for seven consecutive days [17]. After the 7-day induction period of the UC model, all groups were provided normal drinking water and treated for an additional 7 days (from day 7 to day 14) to evaluate drug efficacy. The control and model groups received an equivalent volume of normal saline, while the remaining four groups were orally administered SASP, PGP, Hesp, and the mixture, respectively, for 7 consecutive days (Fig. 1A).

2.3. Pharmacodynamics observation

The severity of UC was evaluated using the disease activity index (DAI) score, a clinical indicator calculated by averaging the scores of weight loss, stool consistency, and stool bleeding. Weight loss was scored as follows: 0 for no weight loss, 1 for 1%–5% weight loss, 2 for 5%–10% weight loss, 3 for 10%–15% weight loss, and 4 for over 15% weight loss. Stool consistency was scored as 0 for normal, 2 for loose stools, and 4 for diarrhea. Stool bleeding was scored as 0 for normal, 2 for hemoccult, and 4 for gross bleeding [18]. Throughout the experiment, body weight, stool consistency, and stool bleeding were recorded daily.

On day 15, all mice were euthanized *via* cervical dislocation. The colons were then carefully dissected, and their lengths were measured and recorded. The spleen and kidneys were photographed and weighed for further analysis. Distal colon tissues were isolated, fixed in 4% paraformaldehyde for 24 h, and subsequently embedded in paraffin. The paraffin-embedded colon samples were sectioned into 4 μm thick slices, stained with haematoxylin and eosin (H&E), and examined under a microscope for histological analysis. Histological scores were evaluated based on previously described criteria [19]. The histological grading scheme was as follows: (i) severity of inflammation: 0, none; 1, slight; 2, moderate; and 3, severe; (ii) inflammatory cell infiltration: 0, none; 1, mucosa; and 2, mucosa and submucosa; and (iii) crypt damage: 0, none; 1, basal one-third damaged; 2, basal two-thirds damaged; 3, only surface epithelium intact; 4, entire crypt and epithelium lost.

2.4. Assessment of oxidative stress

The concentrations of MPO, superoxide dismutase (SOD), and MDA in colon tissue were quantified using commercially

available detection kits [20, 21]. Briefly, colon tissue samples were collected, minced, and homogenized in lysis buffer at a 1∶4 ratio (*W/V*) at 4 °C for 30 min. The homogenates were subsequently centrifuged at 10 000 *g* for 30 min, and the supernatant was collected. After adding the reaction mixture, absorbance at specific wavelengths was measured using an enzyme-labeled instrument, and corresponding concentrations were calculated. The concentration of MDA and the activities of SOD and MPO in the colon were expressed as nmol·mg^{-1} protein, U·g^{-1} protein, and U·g^{-1}, respectively.

2.5. Immunohistochemistry (IHC) and immunofluorescence assay

Colon tissue samples embedded in paraffin were sectioned into 4 μm slices for IHC analysis. The tissue sections underwent dewaxing and rehydration, followed by antigen retrieval through boiling in 10 mmol·L^{-1} citrate buffer for 15 min and blocking endogenous peroxidase with 0.03% H_2O_2 for 10 min. To prevent non-specific binding, the sections were incubated with goat serum at room temperature for 1 h. After blocking, the sections were incubated overnight at 4 °C with primary antibodies against TNF-α (1/200), IL-1β (1/200), IL-10 (1/200), IFN-γ (1/200), IL-4 (1/200), IL-17 (1/200), or TGF-β (1/200), followed by incubation with HRP-conjugated secondary antibodies for 1 h. The antigen-antibody complexes were visualized by staining with diaminobenzidine (DAB), and the sections were counterstained with hematoxylin.

The colon tissue sections for immunofluorescence underwent pretreatment identical to that used for IHC. These sections were then incubated overnight at 4 °C with primary antibodies targeting ZO-1 (1/200), occludin (1/200), and claudin-1 (1/200). Subsequently, the sections were exposed to fluorescent second-

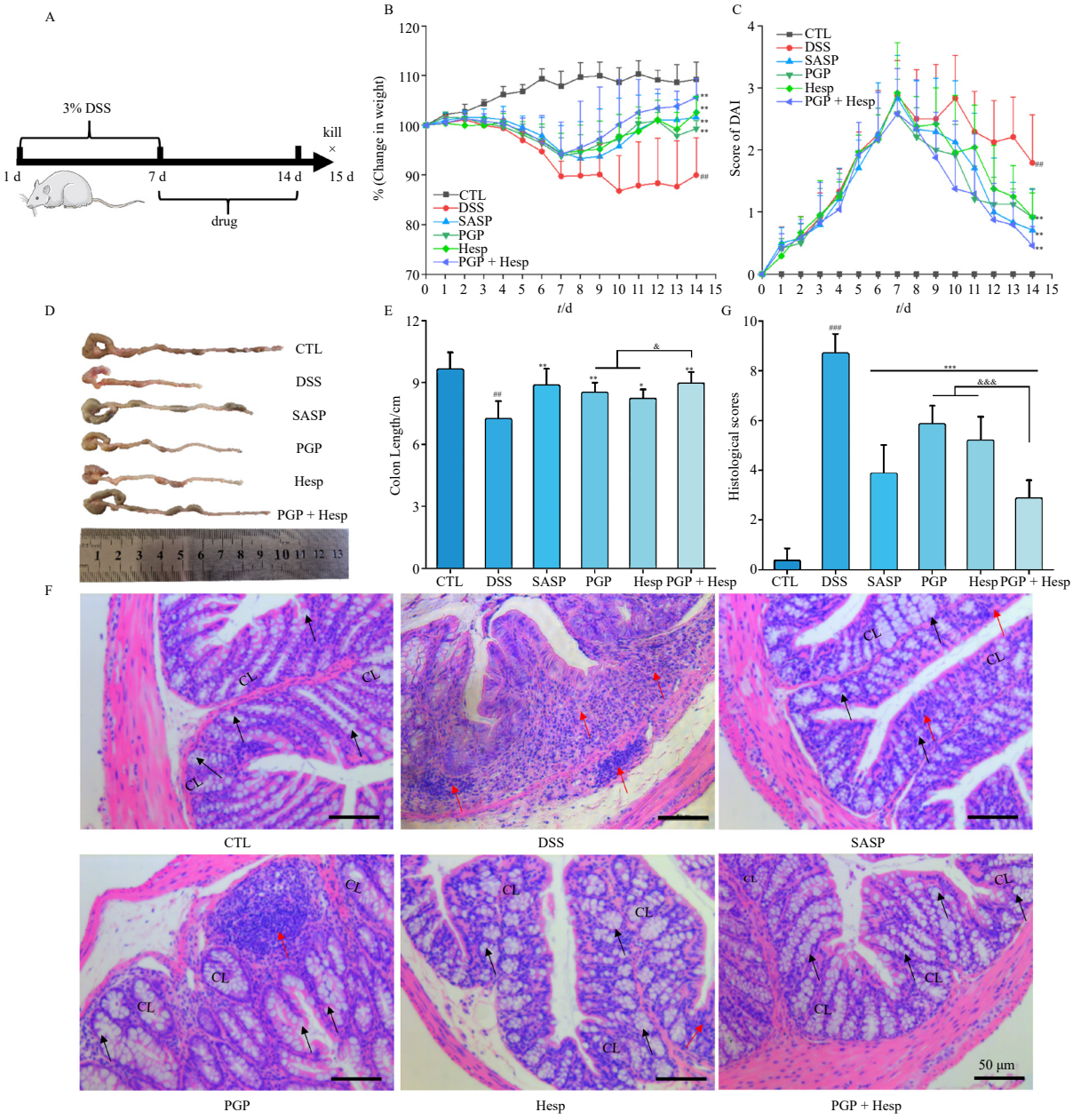

Fig. 1 PGP combined with Hesp ameliorated symptoms in mice with DSS-induced colitis. (A) The experimental design involved drug treatment and induction of colitis using DSS. (B) From day 0 to day 14, alterations in weight were monitored. (C) Recordings of DAI scores were taken between day 0 and day 14. (D) Representative images of the colon were obtained for each group. (E) The colon length was measured for each group. (F, G) Histological (F) and pathological analyses (G) of the colon were performed in DSS-induced colitis mice. CL, crypts of Lieberkühn; the black arrow indicates goblet cells; the red arrow indicates inflammatory cell infiltration. DSS, 3%; SASP, 200 mg·kg^{-1}; PGP, 400 mg·kg^{-1}; Hesp, 80 mg·kg^{-1}; PGP + Hesp, (400 + 80) mg·kg^{-1} (H&E, × 200). Data are presented as mean ± SD (n = 6); $^{*}P < 0.05$, $^{**}P < 0.01$ and $^{***}P < 0.001$ *vs* DSS group; $^{\#\#}P < 0.01$ and $^{\#\#\#}P < 0.001$ *vs* CTL group; $^{\&}P < 0.05$, $^{\&\&\&}P < 0.001$ *vs* PGP + Hesp group.

ary antibodies for 1 h. The process concluded with a 5-min counterstaining using 4',6-diamidino-2-phenylindole (DAPI).

2.6. Reverse transcription-polymerase chain reaction (RT-PCR)

Total RNA was extracted from colon tissue using SparkZol reagent, followed by chloroform extraction and isopropanol precipitation. The RNA concentration was quantified, and complementary deoxyribonucleic acid (cDNA) was synthesized using the M-MLV First-Strand cDNA Synthesis Kit, according to the manufacturer's protocol. After cDNA synthesis, PCR amplification was performed with the Fast HiFidelity PCR Kit and primers designed to target the genes of interest. The primer sequences used in these reactions are provided in Supporting Table [22].

The relative expression of messenger ribonucleic acid (mRNA) was normalized using glyceraldehyde-3-phosphate dehydrogenase (GAPDH) as a reference gene. The mRNA expression levels were quantified by calculating the relative expression ratio in relation to GAPDH expression.

2.7. Terminal deoxynucleotidyl transferase-mediated dUTP nick end labeling (TUNEL)

Apoptosis in colonic tissue was evaluated using the One Step TUNEL Apoptosis Assay Kit (Beyotime Biotechnology, Shanghai, China) according to the manufacturer's protocol. In brief, 4 μm sections of paraffin-embedded colon samples were dewaxed and labeled with TdT-mediated DNA strand breaks using a detection kit. Subsequently, 50 μL of TUNEL detection solution was applied to the samples, which were then incubated at 37 °C in the dark for 1 h. The nucleus was then stained with DAPI [23]. Apoptotic cells were identified by the presence of the green fluorescein marker using a fluorescence microscope. Quantification of TUNEL-positive cells was conducted using ImageJ software for image analysis.

2.8. Cell culture

The RAW264.7 macrophage cell line was obtained from iCell Bioscience (Shanghai, China), while the rat intestinal epithelial cell (IEC) line IEC6 was acquired from Shanghai Zhongqiaoxinzhou Biotech (Shanghai, China). Both cell lines were cultured in Dulbecco's modified Eagle medium (DMEM) supplemented with 10% fetal bovine serum (FBS) and maintained in a humidified incubator at 37 °C with 5% CO_2.

2.9. Cytotoxicity assays

RAW264.7 and IEC6 cells were seeded in 96-well plates at a density of 5×10^3 cells/well and exposed to various concentrations of PGP and Hesp for 24 h, respectively. Each drug concentration was tested in six replicate wells. Following incubation, 10% CCK-8 reagent was added to each well, and the cells were further incubated at 37 °C for 1 h. The optical density (OD) was measured at 450 nm using a microplate reader. The IR was calculated using the formula: percentage of inhibition = [1 − (mean OD of experimental sample/mean OD of the control group)] × 100%. The IC_{50} values, representing the concentration of drug that inhibits cell growth by 50%, were determined [24].

2.10. Drug administration

RAW264.7 and IEC6 cells were categorized into five distinct groups: control, LPS (cells incubated with 2 μg·mL^{-1} LPS for 24 h), LPS + PGP (cells incubated with 2 μg·mL^{-1} LPS and 100 μg·mL^{-1} PGP for 24 h), LPS + Hesp (cells incubated with 2 μg·mL^{-1} LPS and 25 μg·mL^{-1} Hesp for 24 h), and LPS + PGP + Hesp (cells incubated with 2 μg·mL^{-1} LPS, 100 μg·mL^{-1} PGP, and 25 μg·mL^{-1} Hesp for 24 h). Subsequently, the cell culture supernatant was collected, and the nitric oxide (NO) concentration was determined using a Griess reagent kit (Beyotime Biotechnology, Shanghai, China) following the manufacturer's protocol. The levels of TNF-α, IL-1β, and IL-6 in the cell culture supernatant were quantified using ELISA kits.

2.11. Reactive oxygen species (ROS) immunofluorescence

The generation of ROS in IEC6 and RAW264.7 cells was evaluated using the carboxy-2',7'-dichloro-dihydro-fluorescein diacetate (DCFHDA) method [25, 26]. RAW264.7 and IEC6 cells were cultured in 96-well plates (5×10^3 cells/well) or 24-well plates (5×10^4 cells/mL) and subjected to drug treatments as previously described. Following the treatment period, the medium was removed, and the cells were incubated with DCFHDA probes (MedChemExpress, Monmouth Junction, US) for 30 min. The fluorescence intensities were measured at 488 (excitation) and 535 nm (emission) using a microplate reader, and the accumulation of ROS in the cells was visualized through fluorescence microscopy.

2.12. Flow cytometry

The anti-apoptotic effect of the drug was evaluated in RAW264.7 and IEC6 cells using flow cytometry. Cells were inoculated in 6-well plates and treated with drugs as previously described. After removing the supernatant, RAW264.7 and IEC-6 cells were collected and washed three times. Annexin V-fluorescein isothiocyanate (FITC) and PI were used for staining according to the protocol of the apoptosis kit (Solarbio Science & Technology Co, Ltd., Beijing, China). Quantitative assessment of apoptotic cells was performed using flow cytometry.

2.13. Western blot analysis

For Western blot analysis, total proteins were extracted from colon tissues and cell samples using cold RIPA lysis buffer supplemented with PMSF through homogenization on ice. The total protein concentration was quantified using a BCA protein assay kit. Subsequently, proteins were separated by conventional SDS-PAGE and transferred onto a PVDF membrane on ice. Following a 2-h blocking period with 5% skim milk, the membranes were incubated overnight at 4 °C with specific primary antibodies against *β*-actin, claudin-1, occludin, zonula occludens-1 (ZO-1), IL-6, PI3K, AKT, JAK2, STAT3, p-PI3K, p-AKT, p-JAK2, p-STAT3, and PTEN. After washing with tris-buffered saline-Tween 20 (TBST), the protein bands were incubated with a secondary peroxidase-conjugated antibody for 2 h at room temperature. Finally, the membranes were washed with TBST and visualized using an enhanced chemiluminescence reagent. Semi-quantitative analysis was conducted using ImageJ software.

2.14. Statistical analysis

All values are expressed as mean ± SD. Statistical significance was determined using one-way ANOVA followed by LSD post-hoc tests. $^{*}P < 0.05$ was considered statistically significant. $^{**}P < 0.01$ and $^{***}P < 0.001$ were deemed highly significant.

3. Results

3.1. PGP combined with Hesp ameliorated DSS-induced colitis symptom

To induce colitis, a common model of UC in mice, the animals were treated with 3% DSS for 7 d in our study. The effects of PGP,

Hesp, and their combination on DSS-induced colitis were evaluated using weight loss, DAI score, spleen index, colon length, and kidney index. As illustrated in Fig. 1B, the weight of the control (CTL) group steadily increased, whereas that of the DSS group decreased consistently. From the 7th day onward, PGP, Hesp, and their combination were found to mitigate weight loss in mice, comparable to sulfasalazine (SASP). The DAI score, a direct indicator of disease state, increased in mice following DSS induction. Notably, compared to the DSS group, the CTL group, SASP group, treatment groups, and particularly the PGP combined with Hesp group, exhibited a significant decrease in DAI score (Fig. 1C). Furthermore, DSS-induced colonic shortening and renal swelling were observed, while PGP combined with Hesp treatment effectively ameliorated these conditions (Figs. 1D, 1E and S3A). The spleen index, an indirect measure of immune activity, was significantly higher in the DSS group compared to the CTL group, which was effectively reversed by PGP + Hesp treatment (Fig. S3B). Additionally, histological examination of the distal colon tissue using H&E staining revealed that DSS-induced damage, including epithelial layer rupture, loss of goblet cells, and infiltration of inflammatory cells, was significantly repaired in the treatment group (Figs. 1F and 1G). Notably, the PGP + Hesp group showed no significant difference compared to the normal group.

3.2. Effect of PGP combined with Hesp on the expression of tissue inflammatory factors and oxidative stress

Inflammatory injury, characterized by aberrant expression of inflammatory cytokines and excessive oxidative stress, represents a critical pathological process in colitis. As illustrated in Figs. 2A–2D, the expression levels of pro-inflammatory factors TNF-α and IL-1β in the colon tissue of mice in the DSS group were significantly elevated, while the expression of anti-inflammatory factor IL-10 was markedly reduced compared to the CTL group. However, all treatment groups effectively reversed the abnormal expression of inflammatory cytokines, with the PGP + Hesp group demonstrating the most pronounced effect. Furthermore, MPO activity in the colonic tissues of the DSS group was significantly increased and subsequently decreased after treatment (Fig. 2E). SOD and MDA were utilized as indicators of oxidative stress response. The MDA level in colonic tissue of the DSS group was significantly elevated, while SOD activity was notably decreased compared to the CTL group. Nevertheless, other treatment groups successfully reversed the imbalance of SOD and MDA, with the PGP + Hesp group exhibiting the most significant effect (Figs. 2F and 2G).

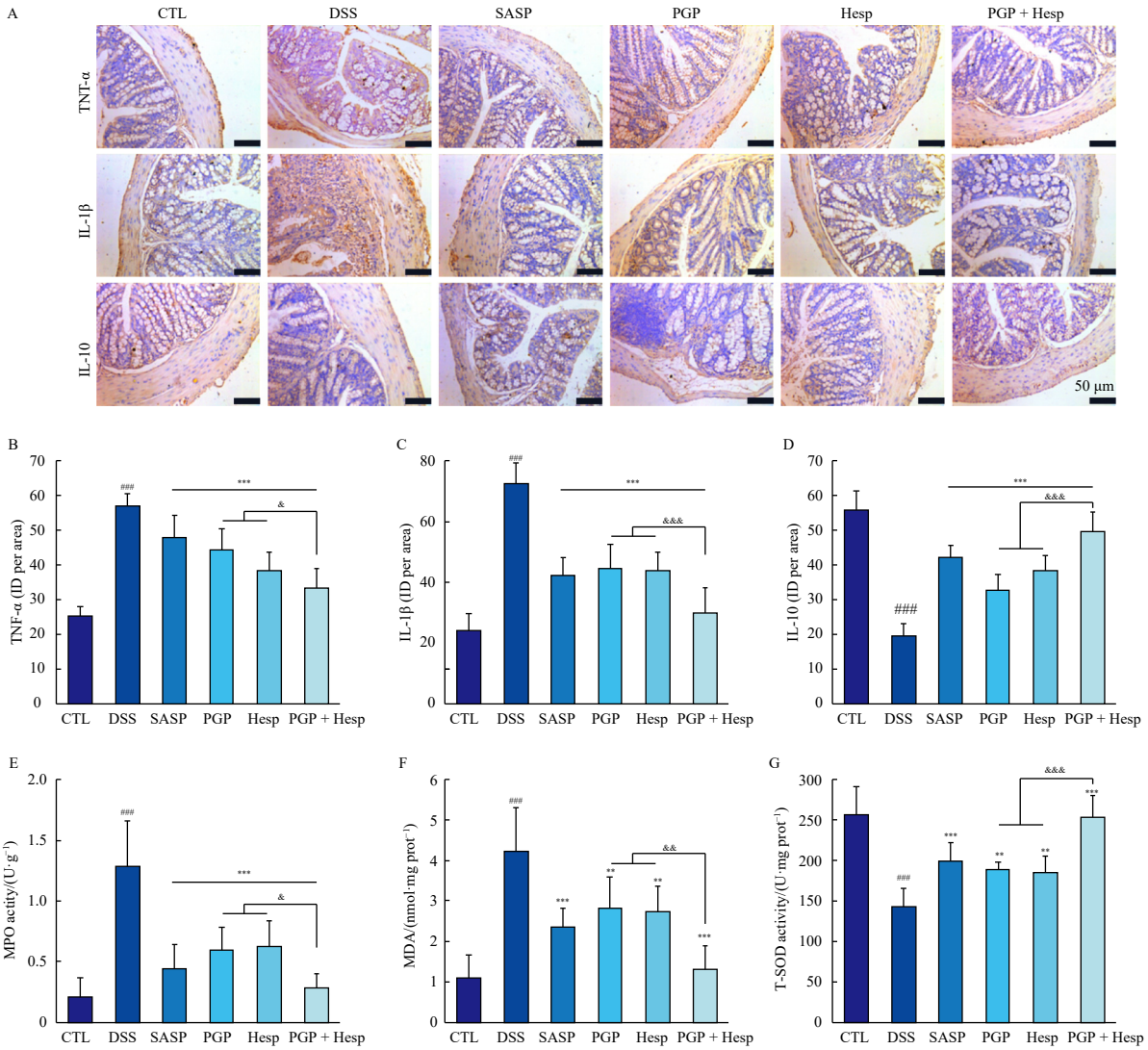

Fig. 2 PGP combined with Hesp alleviated inflammation and oxidative stress induced by DSS in mice. (A) Representative images of TNF-α, IL-1β, and IL-10 staining of the colon tissues. (B–D) The expression of TNF-α (B), IL-1β (C), and IL-10 (D) was analyzed using image analysis. (E–G) The colon tissues were analyzed for MPO (E), MDA (F), and SOD (G) levels. DSS, 3%; SASP, 200 mg·kg^{-1}; PGP, 400 mg·kg^{-1}; Hesp, 80 mg·kg^{-1}; PGP + Hesp, (400 + 80) mg·kg^{-1} (IHC, × 200). Data are presented as mean ± SD (n = 6); $^{**}P$ < 0.01 and $^{***}P$ < 0.001 *vs* DSS group; $^{###}P$ < 0.001 *vs* CTL group; $^{&}P$ < 0.05, $^{&&}P$ < 0.01 and $^{&&&}P$ < 0.001 *vs* PGP + Hesp group.

3.3. Effects of PGP combined with Hesp on Th1, Th2, Th17, and Treg-related cytokines and transcription factors in DSS-induced colitis mice

To investigate the effect of the combination of PGP and Hesp on the Th1/Th2 and Th17/Treg balance in DSS-induced UC mouse colon tissue, we conducted IHC staining to analyze cytokines related to Th1 (IFN-γ), Th2 (IL-4), Th17 (IL-17), and Treg (TGF-β). Additionally, we extracted total mRNA from colon tissue using RT-PCR to analyze transcription factors related to Th1 (T-bet), Th2 (GATA-3), Th17 [retinoic acid-related orphan receptor γt (ROR-γt)], and Treg [Forkhead box P3 (Foxp3)]. The results depicted in Figs. 3A and 3B demonstrate that the administration of PGP and Hesp significantly reduced the abnormal increase of IFN-γ and IL-17 in UC mice, while simultaneously increasing the secretion levels of IL-4 and TGF-β. Furthermore, the mRNA levels of *T-bet* and *ROR-γt* were significantly elevated in the model group, whereas the expression levels of *GATA-3* and *Foxp3* were significantly reduced, which were notably reversed in the administration group. Importantly, the combined administration of PGP and Hesp exhibited a more pronounced efficacy compared to the individual administration of PGP or Hesp. These findings suggest that the combined administration of PGP and Hesp can effectively modulate the expressions of cytokines and related transcription factors associated with Th1, Th2, Th17, and Treg in the colonic tissue of colitis (Figs. 3C and 3D).

3.4. Effects of PGP combined with Hesp on tight junction proteins and apoptosis in colon tissue

Impaired intestinal barrier function leading to increased intestinal permeability is a crucial pathogenic factor in intestinal inflammation. To elucidate the specific protective mechanism of PGP combined with Hesp against DSS colitis, we further evaluated intestinal barrier function. Immunofluorescence analysis revealed that the expression levels of ZO-1, claudin-1, and occludin were significantly downregulated after DSS intervention but were markedly upregulated in the treatment group upon drug administration (Figs. 4A and 4B). Notably, the effects were more pronounced in the PGP + Hesp group than in the groups administered with either drug alone (Figs. 4A and 4B). It is well-established that as colonic mucosal inflammation progresses, there is a substantial increase in apoptotic cell accumulation, which can contribute to severe intestinal diseases if apoptosis becomes dysfunctional or excessive. To assess apoptotic levels in the mouse colon, TUNEL staining was performed. The DSS group exhibited significantly higher levels of apoptosis compared to the CTL group (Fig. 4C). However, drug treatment effectively restored apoptosis to normal levels, with the PGP + Hesp group demonstrating the most significant improvement compared to the model group (Fig. 4C).

3.5. Effects of PGP combined with Hesp on PTEN/PI3K/AKT and IL-6/JAK2/STAT3 signal pathways in colon tissue

To elucidate the mechanism by which PGP combined with Hesp alleviates DSS-induced colitis, we analyzed the relevant IL-6/JAK2/STAT3 and PTEN/PI3K/AKT signaling pathways, which are major inflammatory pathways and signals. In this study, we assessed the protein levels of IL-6, PI3K, AKT, JAK2, STAT3, p-PI3K, p-AKT, p-JAK2, p-STAT3, and PTEN using Western blot analysis (Fig. 5). The results revealed that the combination of PGP and Hesp effectively reduced the levels of p-PI3K, p-AKT, IL-6, p-STAT3, and p-JAK2, while no significant changes were observed in the levels of PI3K, STAT3, AKT, and JAK2. Additionally, the expression level of PTEN protein was significantly increased by the combination treatment (Figs. 5A–5G). Notably, the combined administration of PGP and Hesp demonstrated a more pronounced effect on the relevant signaling pathways, which was comparable to that observed in the normal group, despite the separate administration of PGP and Hesp also showing similar effects.

3.6. Synergistic effects of PGP and Hesp on inhibits LPS-induced inflammation in RAW264.7/IEC6 cells

To assess the anti-inflammatory effect of PGP combined with Hesp *in vitro*, we examined the impact of PGP and Hesp on LPS-induced NO content, inflammatory factor secretion, and oxidative stress in RAW264.7/IEC6 cells. As shown in Fig. S4, we determined the optimal doses of PGP and Hesp to be 100 and 25 $\mu g \cdot mL^{-1}$, respectively. LPS-induced RAW264.7 cells demonstrated a significant increase in NO content and pro-inflammatory factors TNF-α, IL-1β, and IL-6, a decrease in SOD activity, and an increase in MDA level compared to the CTL group (Fig. 6A). Following drug treatment, the levels of these inflammatory cytokines were significantly reduced, and the balance of SOD and MDA was restored, indicating alleviation of LPS-induced inflammation (Fig. 6A). Moreover, the PGP + Hesp group exhibited a more pronounced anti-inflammatory effect than the individual administration groups (Fig. 6A). Similar results were observed in IEC6 cells (Fig. 6B), further supporting the synergistic effect of PGP combined with Hesp in reducing inflammation in UC.

3.7. Synergistic effects of PGP and Hesp in inhibiting ROS accumulation in LPS-induced RAW264.7/IEC6 cells

Upon stimulation, inflammatory cells release various ROS, which can induce cellular and tissue damage, exacerbating inflammatory diseases. Excessive ROS production may also activate signaling pathways involved in the inflammatory process. Consequently, ROS elimination could potentially alleviate inflammation-related conditions. In this context, we investigated the effects of PGP combined with Hesp on LPS-induced ROS. As shown in Fig. 7, LPS-induced RAW264.7 cells exhibited significantly higher ROS fluorescence intensity compared to the control (CTL) group. However, pretreatment with PGP and Hesp, either individually or in combination, significantly reduced this intensity. Notably, the PGP and Hesp combination demonstrated more potent inhibition of LPS-induced ROS than either compound administered individually.

3.8. Synergistic effects of PGP and Hesp in inhibiting apoptosis in LPS-induced RAW264.7/IEC6 cells

To assess apoptosis, Annexin V/PI staining was utilized. As illustrated in Fig. 8A, the apoptosis rate induced by LPS was significantly elevated compared to the CTL group. However, pretreatment with PGP and Hesp individually or in combination resulted in a significant reduction of the apoptosis rate relative to the model group. Notably, the combined administration of PGP and Hesp demonstrated a more potent inhibitory effect on LPS-induced apoptosis than the individual application of PGP or Hesp (Fig. 8A).

3.9. Impact of PGP combined with Hesp on LPS-induced damage to IEC6 tight junction proteins

Further investigation examined the effects of PGP combined with Hesp on cell tight junction proteins at the cellular level. Western blot analysis demonstrated that LPS treatment led to a significant downregulation of tight junction proteins, including ZO-1, claudin, and occludin. In contrast, treatment with PGP and Hesp, both individually and in combination, effectively mitigated this decrease in protein expression (Fig. 8B). Notably, the combined administration of PGP and Hesp exhibited a more pro-

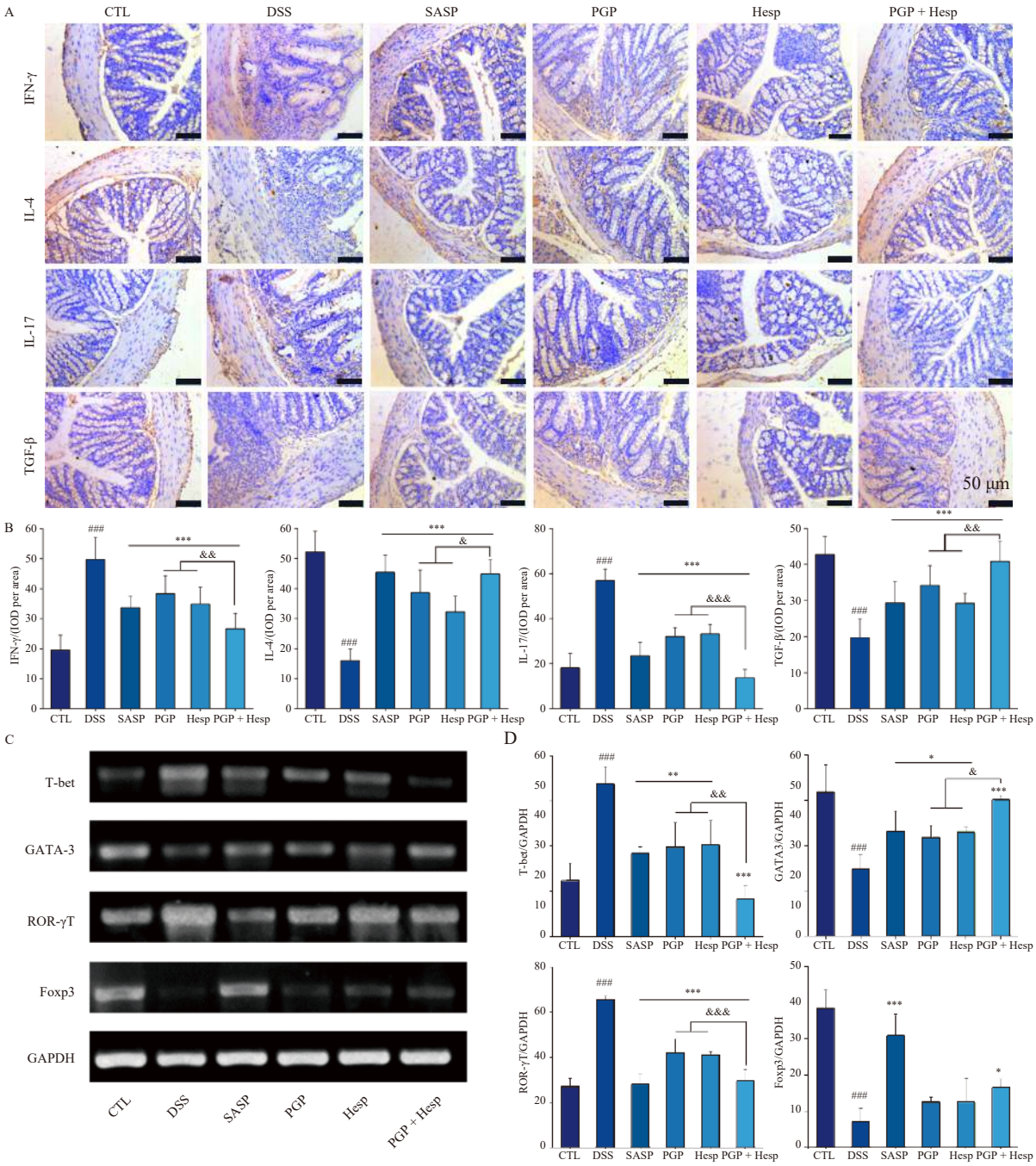

Fig. 3 PGP combined with Hesp regulated the expression of cytokines and transcription factors related to Th1, Th2, Th17, and Treg in colon tissue. (A) Representative images of IFN-γ, IL-4, IL-17, and TGF-β staining of the colon tissues. (B) The expression of related cytokines was analyzed using image analysis. (C) Relative mRNA expression of related transcription factors. (D) Statistics of the related transcription factors. DSS, 3%; SASP, 200 mg·kg^{-1} PGP, 400 mg·kg^{-1}; Hesp, 80 mg·kg^{-1}; PGP + Hesp, (400 + 80) mg·kg^{-1}. IHC, × 200; Data are presented as mean ± SD (n = 6); $^{*}P < 0.05$, $^{**}P < 0.01$ and $^{***}P < 0.001$ *vs* DSS group; $^{\#\#\#}P < 0.001$ *vs* CTL group; $^{\&}P < 0.05$, $^{\&\&}P < 0.01$ and $^{\&\&\&}P < 0.001$ *vs* PGP + Hesp group.

nounced protective effect than either treatment alone (Fig. 8B). Additionally, immunofluorescence analysis of ZO-1 expression corroborated the Western blot results (Fig. 8C).

3.10. Effects of PGP combined with Hesp on LPS-induced PTEN/PI3K/AKT and IL-6/JAK2/STAT3 signaling pathways in RAW264.7/IEC6 cells

To elucidate the mechanism underlying the anti-inflammatory effects of PGP combined with Hesp, this study investigated the impact of this drug combination on the PTEN/PI3K/AKT and IL-6/JAK2/STAT3 signaling pathways at the cellular level. The results are presented in Fig. 9. In LPS-induced RAW264.7/IEC6 cells, the expression levels of p-PI3K, p-STAT3, p-AKT, p-JAK2, and IL-6 were significantly elevated, while the expression level of PTEN was significantly reduced, indicating the activation of the IL-6/JAK2/STAT3 and PTEN/PI3K/AKT signaling pathways. Compared to the administration of each drug alone, the combination significantly decreased the expression levels of p-PI3K, p-STAT3, p-AKT, p-JAK2, and IL-6, and increased the expression level of PTEN. These findings align with the results of animal experiments.

3.11. PGP combined with Hesp synergistically activates PI3K/AKT and JAK2/STAT3 signaling pathways to protect LPS-induced RAW264.7 cells

This study examined the impact of PGP on the PI3K/AKT

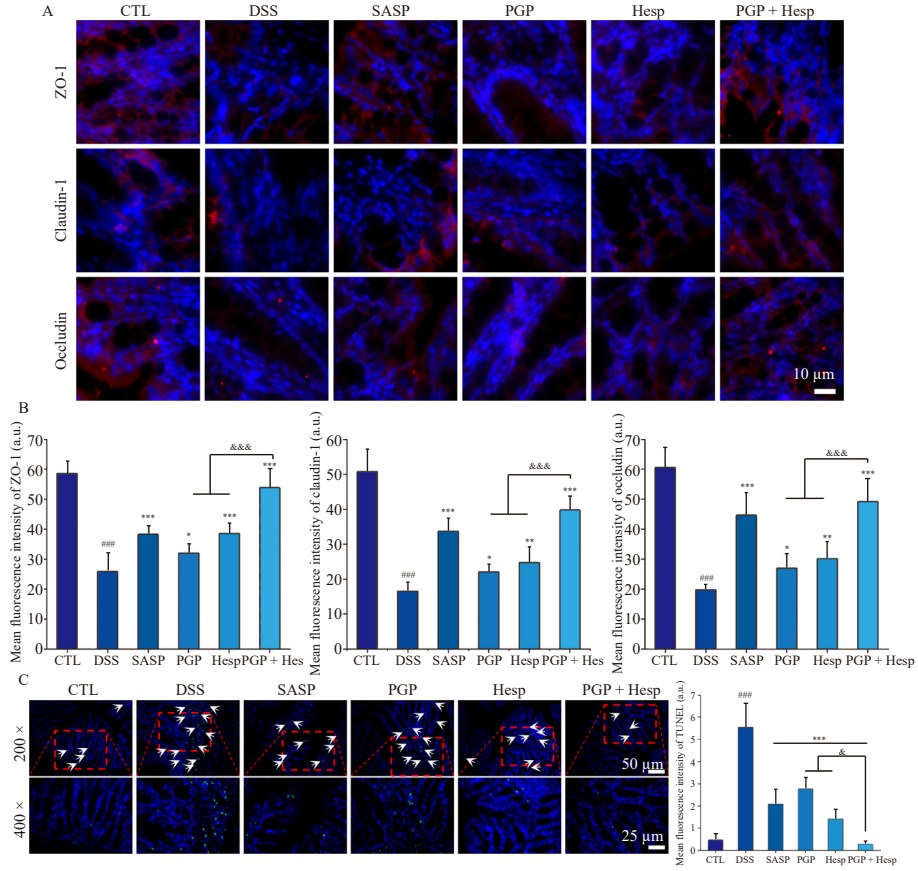

Fig. 4 PGP combined with Hesp was found to enhance the integrity of the mucosal barrier and mitigate DSS-induced apoptosis. (A) Representative images of ZO-1, claudin-1, and occludin staining of the colon tissues. (B) Immunofluorescence analysis of ZO-1, claudin-1, and occludin in the colon tissues. (C) Representative images of TUNEL staining of the colon tissues. DSS, 3%; SASP, 200 mg·kg^{-1}; PGP, 400 mg·kg^{-1}; Hesp, 80 mg·kg^{-1}; PGP + Hesp, (400 + 80) mg·kg^{-1}. IF, × 200; Data are presented as mean ± SD (n = 6); $^{*}P < 0.05$, $^{**}P < 0.01$ and $^{***}P < 0.001$ *vs* DSS group; $^{\#\#\#}P < 0.001$ *vs* CTL group; $^{\&\&\&}P < 0.001$ *vs* PGP + Hesp group.

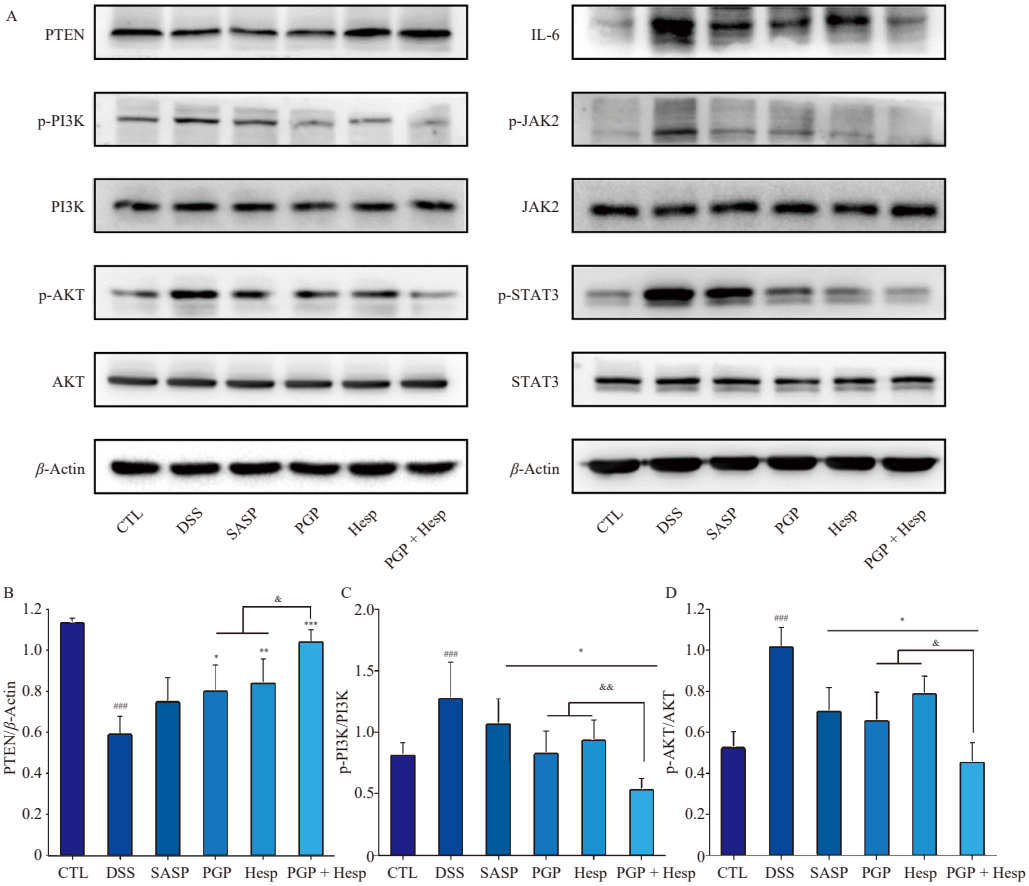

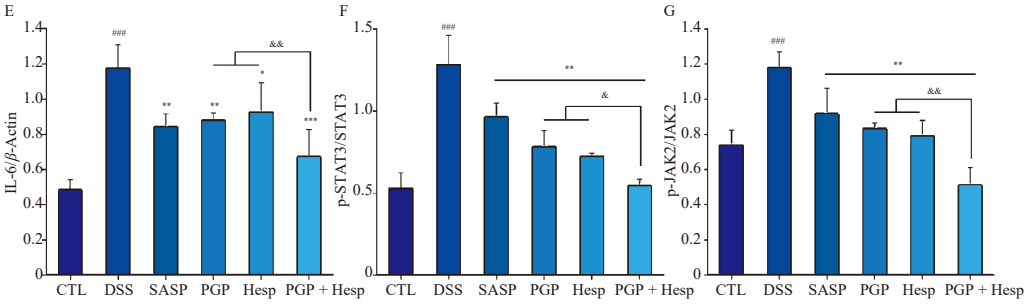

Fig. 5 PGP combined with Hesp ameliorates DSS-induced colitis *via* regulating PTEN/PI3K/AKT and IL-6/JAK2/STAT3 signaling pathways. (A) The protein levels of PTEN, p-PI3K, PI3K, p-AKT, AKT, IL-6, p-JAK2, JAK2, p-STAT3, and STAT3 in the colon were assessed using a Western blot assay. (B–G) Grayscale statistics of PTEN (B), p-PI3K (C), p-AKT (D), IL-6 (E), p-STAT3 (F), and p-JAK2 (G) relative to internal control. DSS, 3%; SASP, 200 mg·kg^{-1}; PGP, 400 mg·kg^{-1}; Hesp, 80 mg·kg^{-1}; PGP + Hesp, (400 + 80) mg·kg^{-1}. Data are presented as mean ± SD (n = 6); $^{*}P < 0.05$, $^{**}P < 0.01$ and $^{***}P < 0.001$ *vs* DSS group; $^{\#\#\#}P < 0.001$ *vs* CTL group; $^{\&}P < 0.05$, $^{\&\&}P < 0.01$ and $^{\&\&\&}P < 0.001$ *vs* PGP + Hesp group.

pathway and Hesp on the JAK2/STAT3 pathway *in vitro*. RAW264.7 cells and IEC6 cells were utilized, with or without LPS challenge, and various concentrations of PGP and Hesp were applied. As shown in Fig. 10A, PGP at different concentrations inhibited the LPS-induced activation of the PI3K/AKT signaling pathway. Likewise, Hesp at varying concentrations inhibited the LPS-

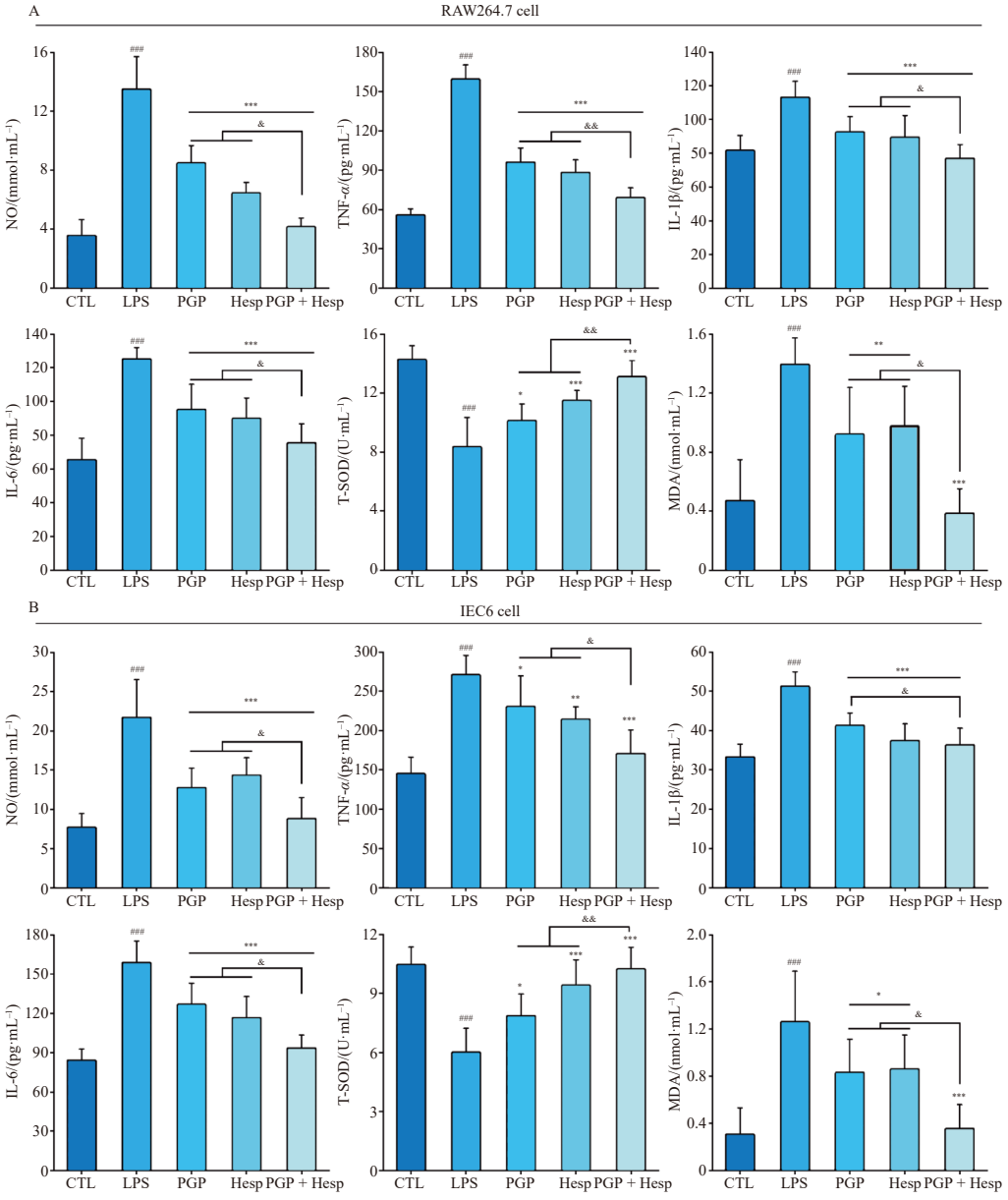

Fig. 6 Effect of PGP combined with Hesp on the inflammation in LPS-induced RAW264.7/IEC6 cells. The anti-inflammatory effects of PGP in combination with Hesp on RAW264.7 cells (A) and IEC6 cells (B) stimulated by LPS were observed respectively. The concentrations of NO, TNF-α, IL-1β, IL-6, T-SOD, and MDA in the culture medium were measured using NO assay kit, ELISA, SOD, and MDA detection kits, respectively. LPS, 2 μg·mL^{-1}; PGP, 100 μg·mL^{-1}; Hesp, 25 μg·mL^{-1}; PGP + Hesp, (100 + 25) μg·mL^{-1}. Data are presented as mean ± SD (n = 6); $^{*}P < 0.05$, $^{**}P < 0.01$ and $^{***}P < 0.001$ *vs* LPS group; $^{\#\#\#}P < 0.001$ *vs* CTL group; $^{\&}P < 0.05$, and $^{\&\&}P < 0.01$ *vs* PGP + Hesp group.

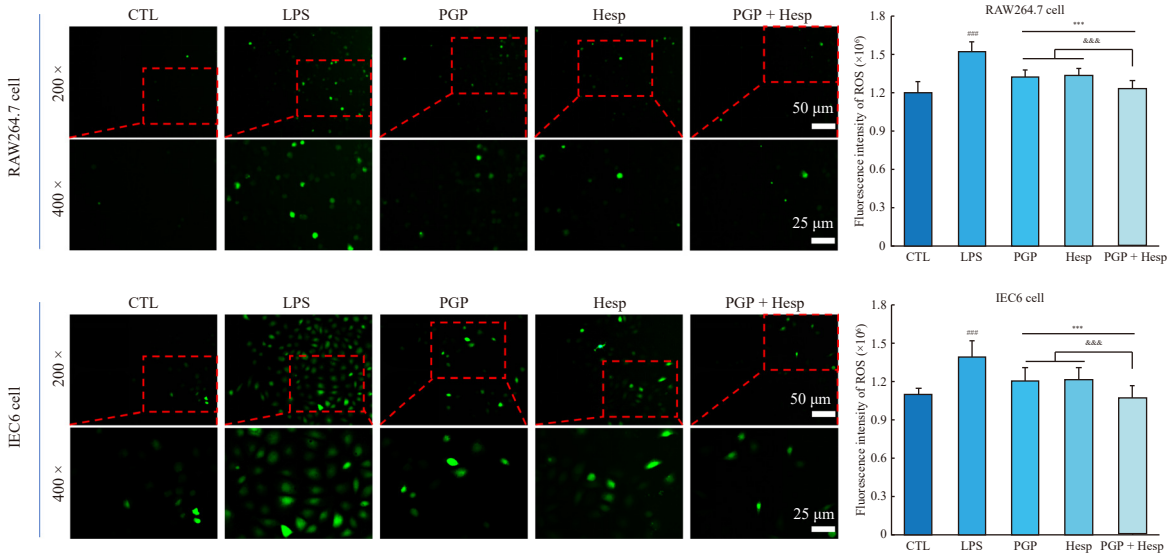

Fig. 7 Effects of PGP combined with Hesp on inhibiting LPS-induced cell production of ROS. The fluorescent probe DCFH-DA was employed to detect ROS in stained cells, and fluorescence microscope images demonstrated the cellular production of ROS. LPS, 2 μg·mL^{-1}; PGP, 100 μg·mL^{-1}; Hesp, 25 μg·mL^{-1}; PGP + Hesp, (100 + 25) μg·mL^{-1}. IF, × 200; Data are presented as mean ± SD (n = 6); $^{***}P < 0.001$ *vs* LPS group; $^{###}P < 0.001$ *vs* CTL group; $^{&&&}P < 0.001$ *vs* PGP + Hesp group.

induced activation of the JAK2/STAT3 signaling pathway. Further investigation focused on the effects of activators and inhibitors of the PI3K/AKT and JAK2/STAT3 signaling pathways, respectively. The results, presented in Fig. S5, demonstrate that treatment with PGP or LY294002 suppressed the LPS-induced activation of the PI3K/AKT signaling pathway in RAW264.7 cells, while treatment with Hesp or AG490 suppressed the LPS-induced activation of the JAK2/STAT3 signaling pathway. These observations indicate that PGP inhibits the activation of the PI3K/AKT signaling pathway, while Hesp inhibits the activation of the JAK2/STAT3 signaling pathway.

To further elucidate the mechanism underlying the anti-inflammatory effects of PGP combined with Hesp, we utilized two pathway activators either individually or in combination. As depicted in Fig. 10B, the combination of LPS and 740 Y-P or Colivelin significantly activated the PI3K/AKT and JAK2/STAT3 signaling pathways compared to the normal group. However, the combination of PGP and Hesp inhibited the activation of both signaling pathways induced by 740 Y-P and Colivelin. Notably, PGP combined with Hesp inhibited the activation of the PI3K/AKT signaling pathway induced by 740 Y-P and the activation of the JAK2/STAT3 signaling pathway induced by Colivelin, respectively. Based on these findings, it can be inferred that a synergistic effect exists between the PI3K/AKT and JAK2/STAT3 signaling pathways. Furthermore, the combined administration of PGP and Hesp exerts a protective effect against LPS-induced inflammation in RAW264.7 cells by synergistically modulating these pathways.

4. Discussion

The combination of PG and CAL has been traditionally utilized in Chinese medicine. CAL aids in expelling external pathogenic factors by supporting the dispersing function of the spleen, while PG facilitates the circulation of lung Qi and enhances the defensive Qi's dispersing function [27, 28]. The compatibility of PG and CAL is evident in Pai-Nong-San (PNS), which is commonly employed in treating various abscesses, dysentery, diarrhea, and intestinal carbuncle, as described in *Synopsis of Prescriptions of the Golden Chamber* [29]. Previous experimental studies have demonstrated that PNS exhibits effective anti-colitis and colon cancer properties [30-34]. Consequently, the combination of PG and CAL, in the context of regulating Qi circulation, is utilized to disperse pathogenic factors and expel pus, not only in the treatment of UC but also in the clinical management of external pathogenic factors. Our experimental findings also indicate that the combination of PGP, an effective component of PG, and Hesp, an effective component of CAL, demonstrates enhanced therapeutic efficacy.

UC has garnered significant attention due to its increasing prevalence, treatment challenges, and elevated cancer risk [35]. While the exact etiology of UC remains elusive, key factors in its progression include an imbalance of pro-inflammatory cytokines, mucosal immune dysfunction, increased permeability, and compromised intestinal barrier function resulting from the inflammatory state [36-39]. The inflammatory process in UC triggers the release of numerous inflammatory mediators (such as TNF-α, IL-1β, and IL-6), exacerbating the accumulation and infiltration of inflammatory cells in colonic tissue, ultimately leading to elevated MPO levels [39, 40]. Upon neutrophil activation, a substantial production of ROS and reactive nitrogen species (RNS) occurs in the intestinal mucosa, inducing oxidative stress, inactivating SOD, and accumulating MDA. These processes aggravate the disease severity by triggering a mucosal immune response [41-43]. Our findings demonstrate that both PGP and Hesp reduced IL-1β, IL-6, and TNF-α levels, with a more pronounced effect observed in the combined administration group. Moreover, the combined treatment exhibits superior inhibitory effects on the elevation of oxidative stress.

The inflammatory state leads to mucosal immune dysfunction, increased permeability, and compromised intestinal barrier function, which are direct and crucial factors in its development [38]. The immune system disturbance of the intestinal mucosa is characterized by an imbalance of Th1/Th2 and Th17/Treg-related transcription factors and cytokines in colonic tissues [22]. Our study demonstrated that DSS-treated mice exhibited elevated levels of Th1 (IL-1β) and Th17 (IL-17) cytokines, coupled with reduced levels of TGF-β cytokines, indicating an imbalance in Th1/Th2 and Th17/Treg-related cytokines during UC development. Notably, the combination treatment effectively restored the cytokine balance. Interestingly, changes in Th1/Th2 and Th17/Treg-associated transcription factors in colonic tissue aligned with the observed cytokine alterations. The epithelial monolayer's integrity is crucial for maintaining proper intestinal barrier function by effectively preventing antigen invasion and abnormal immune responses. Experimental colitis and individuals with colitis often display elevated levels of epithelial apoptosis, which can compromise mucosal barrier integrity, increase mucosal permeability, and indicate epithelial dysfunction [44]. Consequently, inhibiting apoptosis in IECs may facilitate mucosal

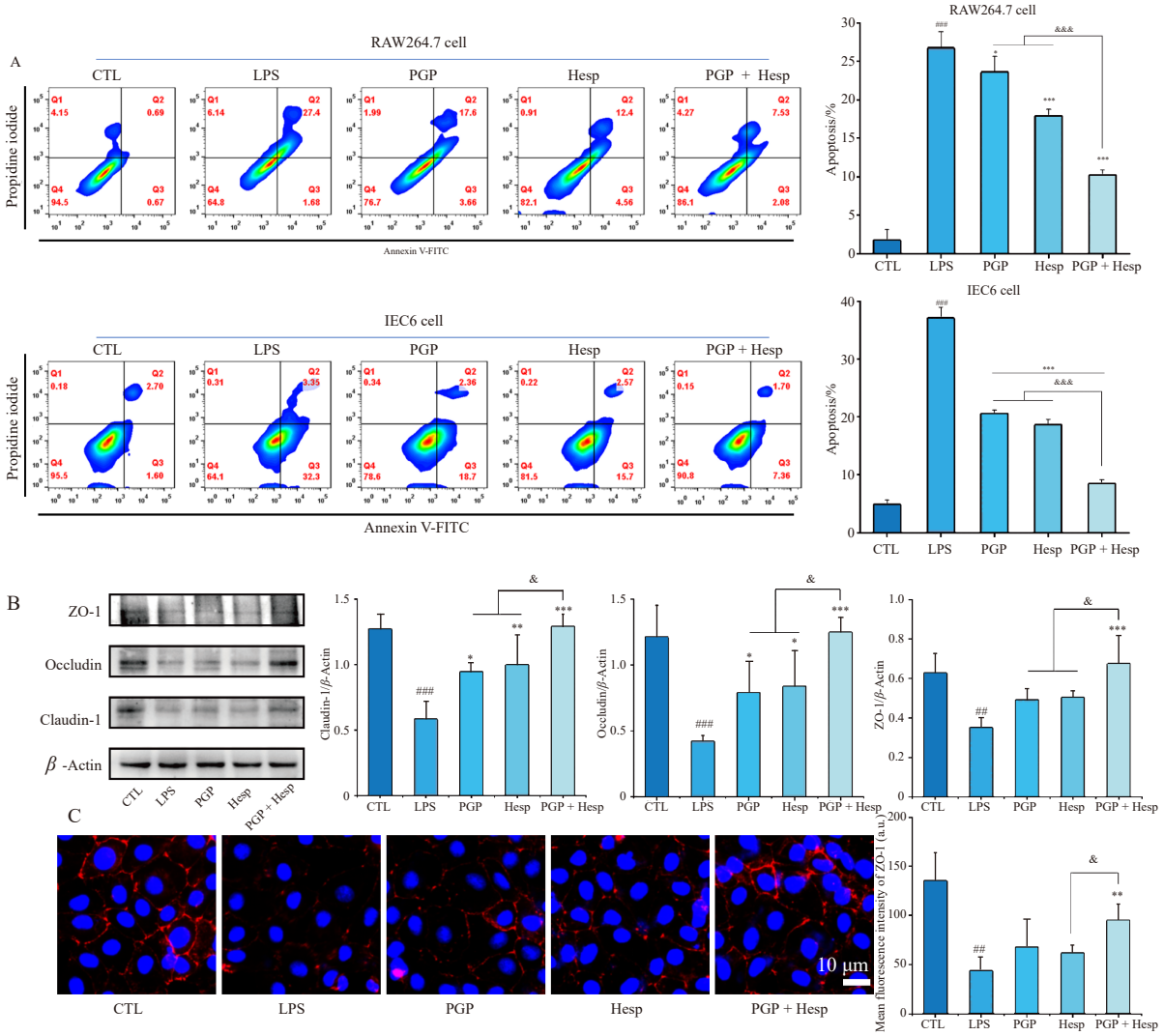

Fig. 8 Effects of PGP combined with Hesp on intestinal barrier dysfunction *in vitro*. (A) The apoptotic data were measured by flow cytometry and expressed as the mean standard deviation. (B) The levels of ZO-1, occludin, and claudin-1 protein were estimated by Western blot. Three specimens were used in the Western blot experiment. (C) Immunofluorescence staining of ZO-1 in the IEC6 cell. LPS, 2 μg·mL^{-1}; PGP, 100 μg·mL^{-1}; Hesp, 25 μg·mL^{-1}; PGP + Hesp, (100 + 25) μg·mL^{-1}. IF, × 200; Data are presented as mean ± SD (n = 3); $^{*}P < 0.05$, $^{**}P < 0.01$ and $^{***}P < 0.001$ *vs* LPS group; $^{\#\#\#}P < 0.001$ *vs* CTL group; $^{\&}P < 0.05$ and $^{\&\&\&}P < 0.001$ *vs* PGP + Hesp group.

healing [45]. The tight junction is a critical factor in regulating the intestinal epithelial barrier and maintaining normal physiological functions. Key components of this structure include tight junction proteins such as ZO-1, claudin-1, and occludin [46].

The PI3K/AKT signaling pathway plays a crucial role in regulating inflammation. Its activation leads to AKT phosphorylation, which subsequently activates NF-κB by enhancing IκB phosphorylation (primarily IκBα) and decreasing IκB synthesis. NF-κB activation promotes TNF-α and IL-1β secretion and expression, resulting in cytokine imbalance, inflammatory cascades, mucosal damage, and ultimately, the onset of UC [47]. Research has shown that the PI3K/AKT pathway regulates oxidative stress levels, and its inhibition can protect DSS-induced colitis mice from oxidative stress-induced damage [48]. Furthermore, this pathway influences T cell survival and activation, playing a vital role in the Th1/Th2 balance *in vivo*. AKT inhibition reduces Th1 cell differentiation. In the presence of a PI3K inhibitor, CD4^{+} T effector cells stimulated *in vitro* exhibit dose-dependent inhibition of cytokine production by Th1, Th2, and Th17 cells, as well as inhibition of Th17 differentiation [49, 50]. Studies have demonstrated that inhibiting the PI3K/AKT pathway can suppress apoptosis, increase tight junction protein expression, and improve intestinal barrier function in rats with UC [51]. Consequently, inhibition of the PI3K/AKT signal transduction pathway can impede NF-κB activation, leading to reduced cytokine release and alleviation of the inflammatory response. This inhibition can also regulate T cell immunity and restore intestinal barrier function, ultimately providing therapeutic benefits for UC treatment.

The JAK/STAT signaling pathway has been implicated in the pathogenesis of UC [52, 53]. STAT3, in particular, plays a crucial role in maintaining IEC function, while its over-activation has been associated with LPS-induced IEC inflammation [54]. Notably, the STAT3 gene has been identified as a susceptibility locus for UC. Under normal conditions, JAK2-mediated phosphorylation of STAT3 at tyrosine 705 (Y705) leads to its activation. The activated STAT3 is then implicated in UC and regulates intestinal immune cell activation [24]. Furthermore, studies have shown that JAK2/STAT3 up-regulation is critical in excessive macrophage activation, resulting in increased pro-inflammatory cytokine secretion, including IL-1β, IL-6, and TNF-α [55]. Concurrently, the JAK/STAT pathway is a key regulator of both cell proliferation and apoptosis [39]. Consequently, inhibition of the JAK2/STAT3 pathway may modulate innate and acquired immune responses and attenuate chronic intestinal inflammation. Clinical trials have explored this approach, employing tofacitinib, a pan-JAK inhibitor, in UC treatment [56, 57].

The activation of the PI3K/AKT and NF-κB signaling pathways can induce the production of TNF-α and IL-6. AKT plays a crucial role in the transcriptional regulation of NF-κB-dependent genes by binding to and activating inhibitors of κB kinase-α

(IKKα), leading to IκB degradation and subsequent NF-κB translocation to the nucleus. This activation of gene transcription ultimately induces IL-6 production [58]. IL-6 activates the JAK2/STAT3 pathway by binding to membrane receptors and activating JAK2, resulting in tyrosine phosphorylation and dimerization of STAT3 monomers. The dimer then translocates to the nucleus and binds to the STAT3-specific DNA response element of target genes, inducing transcription of genes such as *miR-21* [14, 59]. Studies have shown that increased *miR-21* inhibits PTEN expression [60]. PTEN negatively regulates PI3K/AKT signaling by inhibiting PI3K activity through its protein and lipid phosphatase activities. PTEN inhibition may increase PIP3 levels, resulting in PI3K/AKT signal-

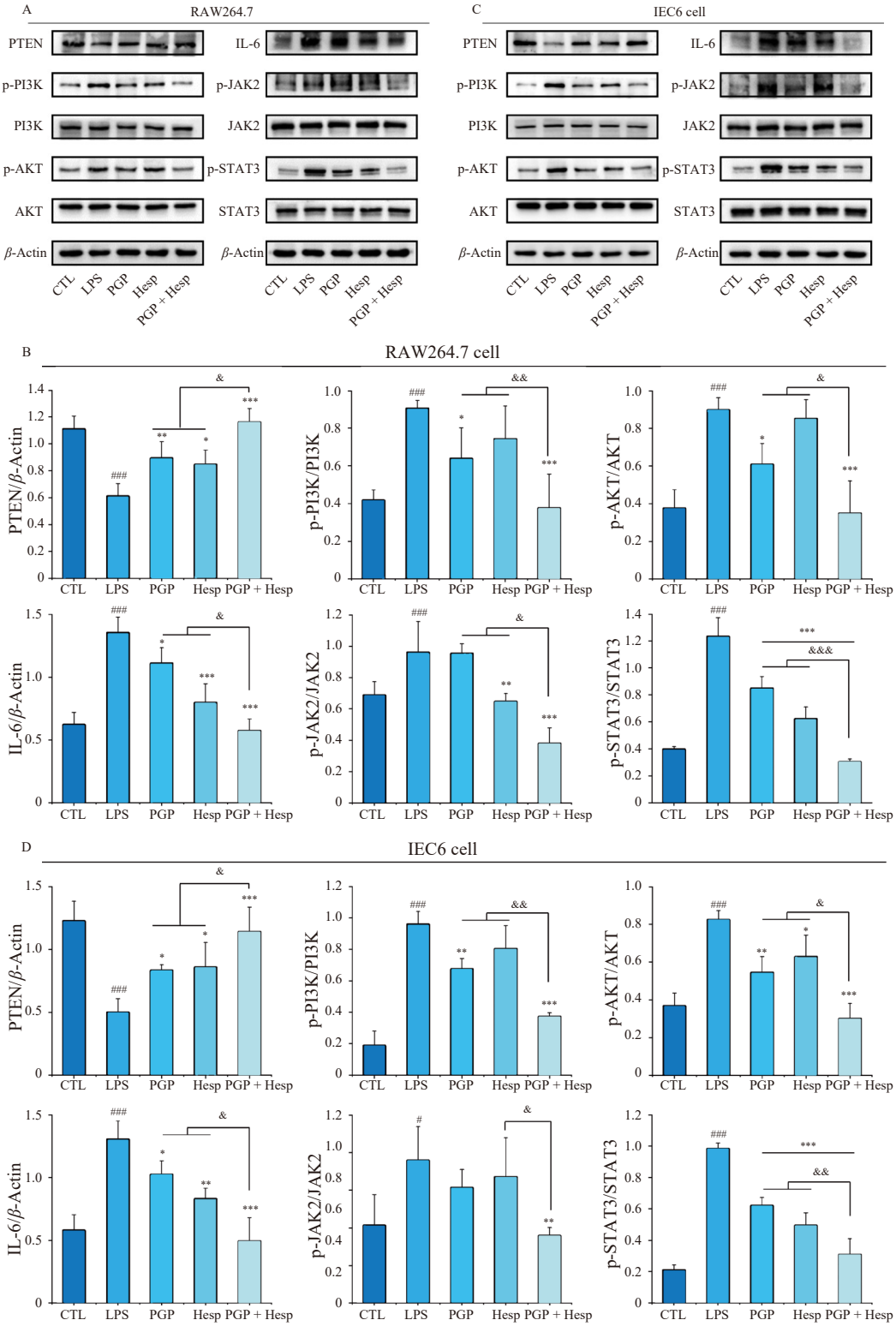

Fig. 9 Effect of PGP combined with Hesp on the PTEN/PI3K/AKT and IL-6/JAK2/STAT3 in LPS-induced RAW264.7/IEC-6 cells. (A, B) Western blot analysis and relative protein expression were performed to determine the protein levels of IPTEN, p-PI3K, PI3K, p-AKT, AKT, IL-6, p-JAK2, JAK2, p-STAT3, and STAT3 in RAW264.7 cells. (C, D) Western blot analysis and relative protein expression were performed to determine the protein levels of IL-6, PI3K, AKT, JAK2, STAT3, p-PI3K, p-AKT, p-JAK2, p-STAT3, and PTEN in IEC6 cells. LPS, 2 μg·mL^{-1}; PGP, 100 μg·mL^{-1}; Hesp, 25 μg·mL^{-1}; PGP + Hesp, (100 + 25) μg·mL^{-1}. Data are presented as mean ± SD (n = 3); $^{*}P < 0.05$, $^{**}P < 0.01$ and $^{***}P < 0.001$ *vs* LPS group; $^{\#}P < 0.05$ and $^{\#\#\#}P < 0.001$ *vs* CTL group; $^{\&}P < 0.05$, $^{\&\&}P < 0.01$ and $^{\&\&\&}P < 0.001$ *vs* PGP + Hesp group.

ing activation [61]. Consequently, PI3K/AKT and JAK2/STAT3 form a positive feedback loop mediated by IL-6 and PTEN (Fig. 11). Our results demonstrate that the combination treatment exhibits superior inhibitory effects on inflammatory factor imbalance, oxidative stress, intestinal mucosal immunity, and intestinal barrier function restoration compared to single treatment groups. Additionally, it more effectively inhibits the activation of PTEN/PI3K/AKT and IL-6/JAK2/STAT3 signaling pathways. Further investigations using specific activators and inhibitors of these signaling pathways revealed that PGP inhibits the PI3K/AKT signaling pathway, while Hesp effectively inhibits the JAK2/STAT3 signaling pathway. To elucidate the underlying anti-inflammatory mechanism of PGP combined with Hesp, we simultaneously activated PI3K/AKT and JAK2/STAT3 signaling pathways using 740 Y-P and Coliverin. The results showed enhanced stimulation of both signals when using 740 Y-P and Coliverin sim-

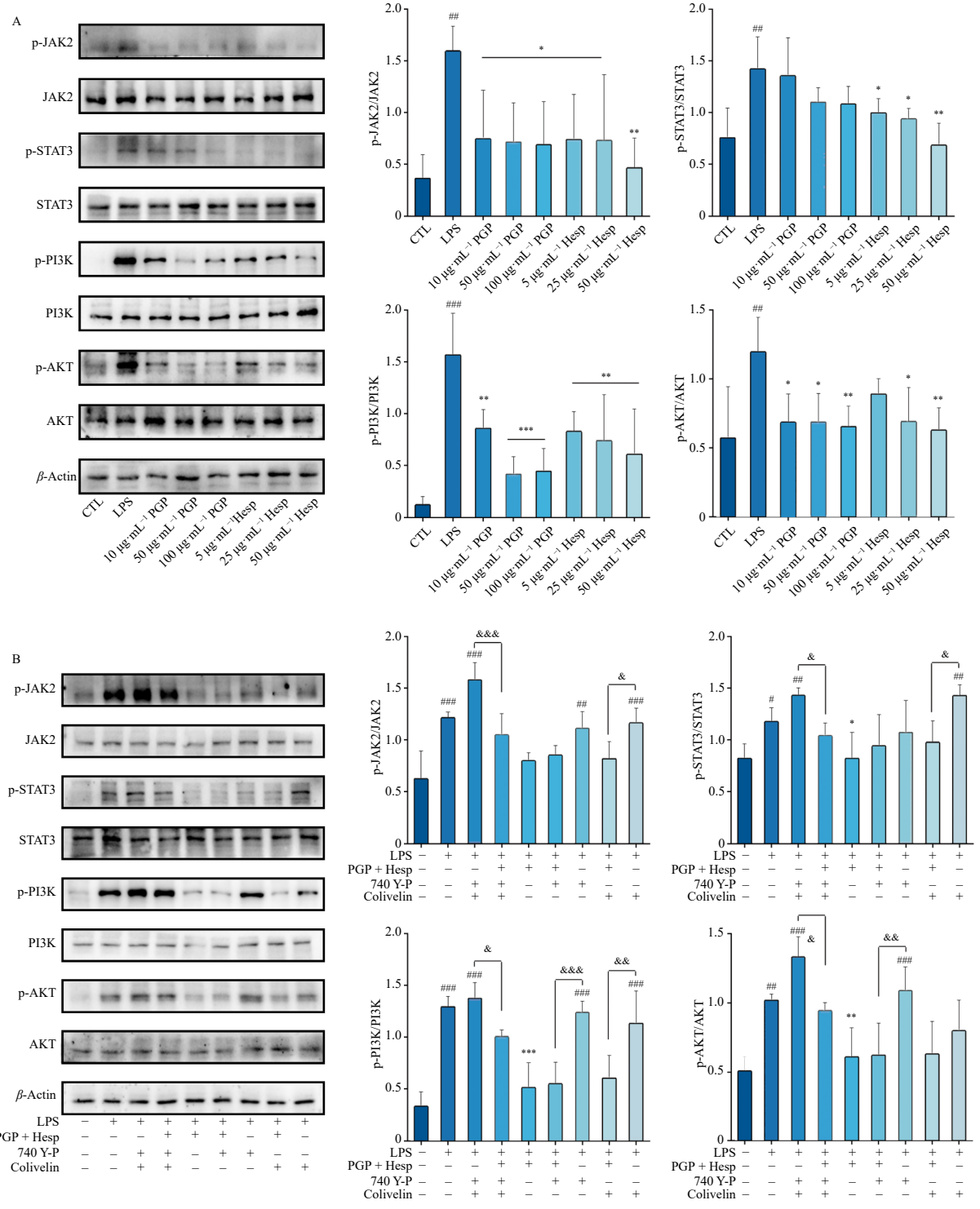

Fig. 10 PGP combined with Hesp synergistically activated the PI3K/AKT and JAK2/STAT3 signaling pathways to protect LPS-induced RAW264.7 cells. (A) RAW264.7 cells were treated with 2 μg·mL^{-1} LPS with or without varying concentrations of PGP (10, 50, 100 μg·mL^{-1} PGP) or Hesp (5, 25, 50 μg·mL^{-1} Hesp) for 24 h. The levels of PI3K, AKT, JAK2, STAT3, p-PI3K, p-AKT, p-JAK2, and p-STAT3 proteins were estimated by Western blot. (B) RAW264.7 cells were treated with 2 μg·mL^{-1} LPS with or without 740 Y-P, Colivelin, or PGP + Hesp for 24 h. The levels of PI3K, AKT, JAK2, STAT3, p-PI3K, p-AKT, p-JAK2, and p-STAT3 proteins were estimated by Western blot. Three specimens were used in the Western blot experiment. LPS, 2 μg·mL^{-1}; PGP, 100 μg·mL^{-1}; Hesp, 25 μg·mL^{-1}; PGP + Hesp, (100 + 25) μg·mL^{-1}. Data are presented as mean ± SD (n = 3); $^{*}P < 0.05$, $^{**}P < 0.01$ and $^{***}P < 0.001$ *vs* LPS group; $^{\#\#}P < 0.01$ and $^{\#\#\#}P < 0.001$ *vs* CTL group; $^{\&}P < 0.05$, $^{\&\&}P < 0.01$ and $^{\&\&\&}P < 0.001$ *vs* PGP + Hesp group.

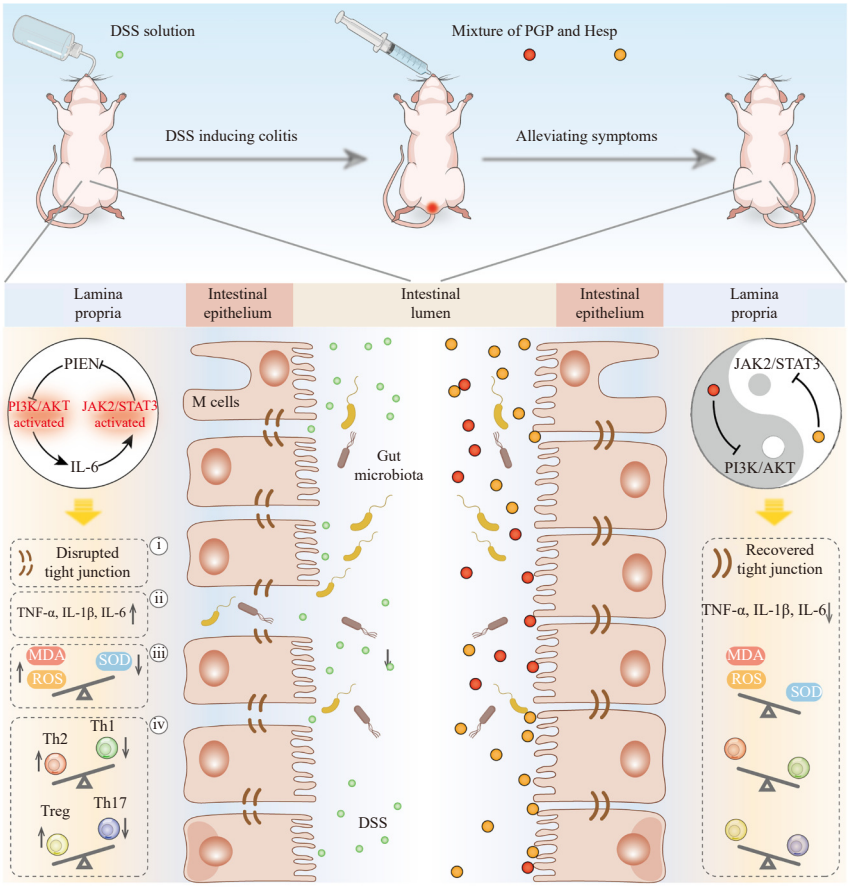

Fig. 11 Synergistic effects of combined PGP with Hesp on PI3K/AKT and JAK2/STAT3 signaling pathway.

ultaneously. However, the combination of drugs inhibited the pathway activator's effect. These findings suggest that the combined anti-inflammatory effect of PGP and Hesp may be attributed to the modulation of the PTEN/PI3K/AKT and IL-6/JAK2/STAT3 signaling pathways.

5. Conclusion

In conclusion, this study demonstrates the synergistic interaction between PGP compounds and Hesp in both DSS-induced colitis in mice and LPS-induced RAW264.7/IEC6 cells. These effects are mediated through multiple mechanisms, including the regulation of inflammatory cytokines, attenuation of oxidative stress, modulation of intestinal mucosal immunity, and the restoration of intestinal barrier integrity. The underlying therapeutic action appears to involve the coordinated modulation of the PTEN/PI3K/AKT and IL-6/JAK2/STAT3 signaling pathways. These findings highlight the potential of combination therapies as a promising strategy for the development of synergistic treatments for complex diseases, such as ulcerative colitis (UC), paving the way for novel therapeutic approaches in clinical settings.

Funding

This work was supported by the Major Fund Project of Anhui Province Department of Education (No. 2022AH040077), the Academic Funding for Top Talents in Disciplines (Specialities) of Anhui Provincial High Education Institutes (No. gxbjZD2021056), and the Program for New Era Cultivate Talents of Anhui province (Postgraduate Education) (No. 2022xscx099).

Supporting information

Supporting information for this work can be obtained by contacting the corresponding authors *via* E-mail.

Declaration of competing interest

All authors declare that they have no conflicts of interest.

References

1 Ordas I, Eckmann L, Talamini M, et al. Ulcerative colitis. *Lancet*. 2012;380(9853):1606-1619. https://doi.org/10.1016/S0140-6736(12)60150-0.
2 Feuerstein JD, Moss AC, Farraye FA. Ulcerative colitis. *Mayo Clin Proc*. 2019;94(7):1357-1373. https://doi.org/10.1016/j.mayocp.2019.01.018.
3 Segal JP, LeBlanc JF, Hart AL. Ulcerative colitis: an update. *Clin Med (Lond)*. 2021;21(2):135-139. https://doi.org/10.7861/clinmed.2021-0080.
4 Pasvol TJ, Horsfall L, Bloom S, et al. Incidence and prevalence of inflammatory bowel disease in UK primary care: a population-based cohort study. *BMJ Open*. 2020;10(7):e036584. https://doi.org/10.1136/bmjopen-2019-036584.
5 Du L, Ha C. Epidemiology and pathogenesis of ulcerative colitis. *Gastroenterol Clin North Am*. 2020;49(4):643-654. https://doi.org/10.1016/j.gtc.2020.07.005.
6 Kucharzik T, Koletzko S, Kannengiesser K, et al. Ulcerative colitis-diagnostic and therapeutic algorithms. *Dtsch Arztebl Int*. 2020;117(33-34):564-574. https://doi.org/10.3238/arztebl.2020.0564.
7 Liu Y, Li BG, Su YH, et al. Potential activity of traditional Chinese medicine against ulcerative colitis: a review. *J Ethnopharmacol*. 2022;289:115084. https://doi.org/10.1016/j.jep.2022.115084.
8 Wang C, Cheng G, Yang S, et al. Protective effects of *Platycodon grandiflorus* polysaccharides against apoptosis induced by carbonyl cyanide 3-chlorophenylhydrazone in 3D4/21 cells. *Int J Biol Macromol*. 2019;141:1220-1227. https://doi.org/10.1016/j.ijbiomac.2019.09.086.
9 Liu Y, Rui XL, Li JC, et al. Effect of *Platycodon grandiflorus* polysaccharide on ulcerative colitis in mice. *Chin Trad Patent Med*. 2022;44(4):1093-1099. https://doi.org/10.3969/j.issn.1001-1528.2022.04.010.
10 Liu Y, Chen Q, Ren R, et al. *Platycodon grandiflorus* polysaccharides deeply participate in the anti-chronic bronchitis effects of *Platycodon grandiflorus* decoction, a representative of "the lung and intestine are related". *Front Pharmacol*. 2022;13:927384. https://doi.org/10.3389/fphar.2022.927384.
11 He W, Li Y, Liu M, et al. *Citrus aurantium* L. and its flavonoids regulate TNBS-induced inflammatory bowel disease through anti-inflammation and suppressing isolated jejunum contraction. *Int J Mol Sci*. 2018;19(10):3057. https://doi.org/10.3390/ijms19103057.

12 Guo K, Ren J, Gu G, et al. Hesperidin protects against intestinal inflammation by restoring intestinal barrier function and up-regulating Treg cells. *Mol Nutr Food Res*. 2019;63(11):e1800975. https://doi.org/10.1002/mnfr.201800975.

13 Elhennawy MG, Abdelaleem EA, Zaki AA, et al. Cinnamaldehyde and hesperetin attenuate TNBS-induced ulcerative colitis in rats through modulation of the JAk2/STAT3/SOCS3 pathway. *J Biochem Mol Toxicol*. 2021;35(5):e22730. https://doi.org/10.1002/jbt.22730.

14 Lai CY, Yeh KY, Liu BF, et al. MicroRNA-21 plays multiple oncometabolic roles in colitis-associated carcinoma and colorectal cancer *via* the PI3K/AKT, STAT3, and PDCD4/TNF-alpha signaling pathways in zebrafish. *Cancers (Basel)*. 2021;13(21):5565. https://doi.org/10.3390/cancers13215565.

15 Seavey MM, Lu LD, Stump KL, et al. Therapeutic efficacy of CEP-33779, a novel selective JAK2 inhibitor, in a mouse model of colitis-induced colorectal cancer. *Mol Cancer Ther*. 2012;11(4):984-993. https://doi.org/10.1158/1535-7163.MCT-11-0951.

16 Liu Y, Dong YH, Shen W, et al. *Platycodon grandiflorus* polysaccharide regulates colonic immunity through mesenteric lymphatic circulation to attenuate ulcerative colitis. *Chin J Nat Med*. 2023;20(4):263-278. https://doi.org/10.1016/S1875-5364(22)60261-9.

17 Xu B, Huang S, Chen Y, et al. Synergistic effect of combined treatment with baicalin and emodin on DSS-induced colitis in mouse. *Phytother Res*. 2021;35(10):5708-5719. https://doi.org/10.1002/ptr.7230.

18 Luo S, Deng X, Liu Q, et al. Emodin ameliorates ulcerative colitis by the flagellin-TLR5 dependent pathway in mice. *Int Immunopharmacol*. 2018;59:269-275. https://doi.org/10.1016/j.intimp.2018.04.010.

19 Lv Q, Wang K, Qiao SM, et al. Norisoboldine, a natural aryl hydrocarbon receptor agonist, alleviates TNBS-induced colitis in mice, by inhibiting the activation of NLRP3 inflammasome. *Chin J Nat Med*. 2018;16(3):161-174. https://doi.org/10.1016/S1875-5364(18)30044-X.

20 Zhou R, Huang K, Chen S, et al. Zhilining Formula alleviates DSS-induced colitis through suppressing inflammation and gut barrier dysfunction *via* the AHR/NF-κBp65 axis. *Phytomedicine*. 2024;129:155571. https://doi.org/10.1016/j.phymed.2024.155571.

21 Li H, Fan C, Feng C, et al. Inhibition of phosphodiesterase-4 attenuates murine ulcerative colitis through interference with mucosal immunity. *Br J Pharmacol*. 2019;176(13):2209-2226. https://doi.org/10.1111/bph.14667.

22 Chen YF, Zheng JJ, Qu C, et al. *Inonotus obliquus* polysaccharide ameliorates dextran sulphate sodium induced colitis involving modulation of Th1/Th2 and Th17/Treg balance. *Artif Cells Nanomed Biotechnol*. 2019;47(1):757-766. https://doi.org/10.1080/21691401.2019.1577877.

23 Wu MY, Liu L, Wang EJ, et al. PI3KC3 complex subunit NRBF2 is required for apoptotic cell clearance to restrict intestinal inflammation. *Autophagy*. 2021;17(5):1096-1111. https://doi.org/10.1080/15548627.2020.1741332.

24 Yu T, Li Z, Xu L, et al. Anti-inflammation effect of Qingchang Suppository in ulcerative colitis through JAK2/STAT3 signaling pathway *in vitro* and *in vivo*. *J Ethnopharmacol*. 2021;266:113442. https://doi.org/10.1016/j.jep.2020.113442.

25 Gutierrez RMP, Hoyo-Vadillo C. Anti-inflammatory potential of *Petiveria alliacea* on activated RAW264.7 murine macrophages. *Pharmacogn Mag*. 2017;13(Suppl 2):S174-S178. https://doi.org/10.4103/pm.pm_479_16.

26 Aranda A, Sequedo L, Tolosa L, et al. Dichloro-dihydro-fluorescein diacetate (DCFH-DA) assay: a quantitative method for oxidative stress assessment of nanoparticle-treated cells. *Toxicol In Vitro*. 2013;27(2):954-963. https://doi.org/10.1016/j.tiv.2013.01.016.

27 Yin PJ, Qu Y. Compatibility and application rules of Jiegeng (Platycodonis Radix) in classical prescriptions. *J Shandong Univ TCM*. 2018;42(6):484-487. https://doi.org/10.16294/j.cnki.1007-659x.2018.06.004.

28 Wang Q, Qu Y. Compatibility and application rules of Zhishi (*Citrus aurantium* L.) in classical prescriptions. *J Guangzhou Univ TCM*. 2018;35(2):374-378. https://doi.org/10.13359/j.cnki.gzxbtcm.2018.02.036.

29 Zhang ZJ. Effects of Painong Powder on acute suppurative disease. *Foreign Med Sci Tradit Chin Med*. 1994;3:29.

30 Zhang MM, Rui XL, Yang Y, et al. Anti-tumor effects of Painong Powder on mice with colon cancer. *Chin Trad Patent Med*. 2021;43(4): 882-887.

31 Zhang MM, Yin DK, Rui XL, et al. Protective effect of Pai-Nong-San against AOM/DSS-induced CAC in mice through inhibiting the Wnt signaling pathway. *Chin J Nat Med*. 2021;19(12):912-920. https://doi.org/10.1016/S1875-5364(22)60143-2.

32 Wang K, Guo J, Chang X, et al. Painong-San extract alleviates dextran sulfate sodium-induced colitis in mice by modulating gut microbiota, restoring intestinal barrier function and attenuating TLR4/NF-κB signaling cascades. *J Pharm Biomed Anal*. 2022;209:114529. https://doi.org/10.1155/2021/2810915.

33 Rui XL, Li JC, Zhang MM, et al. Therapeutic effect of Painong Powder on dextran sodium sulfate-induced colitis mice. *Chin J Mod Appl Pharm*. 2021;38:2940-2944. https://doi.org/10.13748/j.cnki.issn1007-7693.2021.23.005.

34 Li J, Rui X, Xu L, et al. Enhanced therapeutic effect on colitis with powder formulations of Painong San associated with the promotion of intestinal adhesion and absorption. *J Ethnopharmacol*. 2022;289:115030. https://doi.org/10.1016/j.jep.2022.115030.

35 Laharie D. Towards therapeutic choices in ulcerative colitis. *Lancet*. 2017;390(10090):98-99. https://doi.org/10.1016/S0140-6736(17)31263-1.

36 Liang J, Chen S, Chen J, et al. Therapeutic roles of polysaccharides from *Dendrobium officinaleon* colitis and its underlying mechanisms. *Carbohydr Polym*. 2018;185:159-168. https://doi.org/10.1016/j.carbpol.2018.01.013.

37 Luo S, Wen R, Wang Q, et al. Rhubarb Peony Decoction ameliorates ulcerative colitis in mice by regulating gut microbiota to restoring Th17/Treg balance. *J Ethnopharmacol*. 2019;231:39-49. https://doi.org/10.1016/j.jep.2018.08.033.

38 Li J, Ma Y, Li X, et al. Fermented Astragalus and its metabolites regulate inflammatory status and gut microbiota to repair intestinal barrier damage in dextran sulfate sodium-induced ulcerative colitis. *Front Nutr*. 2022;9:1035912. https://doi.org/10.3389/fnut.2022.1035912.

39 Lu Z, Xiong W, Xiao S, et al. Huanglian Jiedu Decoction ameliorates DSS-induced colitis in mice *via* the JAK2/STAT3 signalling pathway. *Chin Med*. 2020;15:45. https://doi.org/10.1186/s13020-020-00327-9.

40 Pavan E, Damazo AS, Arunachalam K, et al. *Copaifera malmei* Harms leaves infusion attenuates TNBS-ulcerative colitis through modulation of cytokines, oxidative stress and mucus in experimental rats. *J Ethnopharmacol*. 2021;267:113499. https://doi.org/10.1016/j.jep.2020.113499.

41 Naito Y, Takagi T, Yoshikawa T. Neutrophil-dependent oxidative stress in ulcerative colitis. *J Clin Biochem Nutr*. 2007;41(1):18-26. https://doi.org/10.3164/jcbn.2007003.

42 Yao J, Wang JY, Liu L, et al. Anti-oxidant effects of resveratrol on mice with DSS-induced ulcerative colitis. *Arch Med Res*. 2010;41(4):288-294. https://doi.org/10.1016/j.arcmed.2010.05.002.

43 Piechota-Polanczyk A, Fichna J. Review article: the role of oxidative stress in pathogenesis and treatment of inflammatory bowel diseases. *Naunyn Schmiedebergs Arch Pharmacol*. 2014;387(7):605-620. https://doi.org/10.1007/s00210-014-0985-1.

44 Mankertz J, Schulzke JD. Altered permeability in inflammatory bowel disease: pathophysiology and clinical implications. *Curr Opin Gastroenterol*. 2007;23(4):379-383. https://doi.org/10.1097/MOG.0b013e32816aa392.

45 Lee Y, Sugihara K, Gillilland MG, et al. Hyaluronic acid-bilirubin nanomedicine for targeted modulation of dysregulated intestinal barrier, microbiome and immune responses in colitis. *Nat Mater*. 2020;19(1):118-126. https://doi.org/10.1038/s41563-019-0462-9.

46 Niu MM, Guo HX, Cai JW, et al. *Bifidobacterium breve* alleviates DSS-induced colitis in mice by maintaining the mucosal and epithelial barriers and modulating gut microbes. *Nutrients*. 2022;14(18):3671. https://doi.org/10.3390/nu14183671.

47 Huang XL, Xu J, Zhang XH, et al. PI3K/Akt signaling pathway is involved in the pathogenesis of ulcerative colitis. *Inflamm Res*. 2011;60(8):727-734. https://doi.org/10.1007/s00011-011-0325-6.

48 Yan S, Hui Y, Li J, et al. Glutamine relieves oxidative stress through PI3K/Akt signaling pathway in DSS-induced ulcerative colitis mice. *Iran J Basic Med Sci*. 2020;23(9):1124-1129. https://doi.org/10.22038/ijbms.2020.39815.9436.

49 Dou D, Liang J, Zhai X, et al. Oxytocin signalling in dendritic cells regulates immune tolerance in the intestine and alleviates DSS-induced colitis. *Clin Sci (Lond)*. 2021;135(4):597-611. https://doi.org/10.1042/CS20201438.

50 Way EE, Trevejo-Nunez G, Kane LP, et al. Dose-dependent suppression of cytokine production from T cells by a novel phosphoinositide 3-kinase delta inhibitor. *Sci Rep*. 2016;6:30384. https://doi.org/10.1038/srep30384.

51 Lu QG, Zeng L, Li XH, et al. Protective effects of *Panax notoginseng* saponin on dextran sulfate sodium-induced colitis in rats through phosphoinositide-3-kinase protein kinase B signaling pathway inhibition. *World J Gastroenterol*. 2020;26(11):1156-1171. https://doi.org/10.3748/wjg.v26.i11.1156.

52 Wang L, Hu Y, Song B, et al. Targeting JAK/STAT signaling pathways in treatment of inflammatory bowel disease. *Inflamm Res*. 2021;70(7):753-764. https://doi.org/10.1007/s00011-021-01482-x.

53 Salas A, Hernandez-Rocha C, Duijvestein M, et al. JAK-STAT pathway targeting for the treatment of inflammatory bowel disease. *Nat Rev Gastroenterol Hepatol*. 2020;17(6):323-337. https://doi.org/10.1038/s41575-020-0273-0.

54 Dambacher J, Beigel F, Seiderer J, et al. Interleukin 31 mediates MAP kinase and STAT1/3 activation in intestinal epithelial cells and its expression is upregulated in inflammatory bowel disease. *Gut*. 2007;56(9):1257-1265. https://doi.org/10.1136/gut.2006.118679.

55 Li L, Xu T, Huang C, et al. NLRC5 mediates cytokine secretion in RAW264.7 macrophages and modulated by the JAK2/STAT3 pathway. *Inflammation*. 2014;37(3):835-847. https://doi.org/10.1007/s10753-013-9804-y.

56 Fernandez-Clotet A, Castro-Poceiro J, Panes J. Tofacitinib for the treatment of ulcerative colitis. *Expert Rev Clin Immunol*. 2018;14(11):881-892. https://doi.org/10.1080/1744666X.2018.1532291.

57 Zhao Y, Luan H, Jiang H, et al. Gegen Qinlian decoction relieved DSS-induced ulcerative colitis in mice by modulating Th17/Treg cell homeostasis *via* suppressing IL-6/JAK2/STAT3 signaling. *Phytomedicine*. 2021;84:153519. https://doi.org/10.1016/j.phymed.2021.153519.

58 Jiang R, Tang J, Zhang X, et al. CCN1 promotes inflammation by inducing IL-6 production *via* alpha6beta1/PI3K/Akt/NF-kappaB pathway in autoimmune hepatitis. *Front Immunol*. 2022;13:810671. https://doi.org/10.3389/fimmu.2022.810671.

59 Huang B, Lang X, Li X. The role of IL-6/JAK2/STAT3 signaling pathway in cancers. *Front Oncol*. 2022;12:1023177. https://doi.org/10.3389/fonc.2022.1023177.

60 Nguyen TT, Ung TT, Li S, et al. Lithocholic acid induces miR21, promoting PTEN inhibition *via* STAT3 and ERK-1/2 signaling in colorectal cancer cells. *Int J Mol Sci*. 2021;22(19):10209. https://doi.org/10.3390/ijms221910209.

61 Tokuhira N, Kitagishi Y, Suzuki M, et al. PI3K/AKT/PTEN pathway as a target for Crohn's disease therapy (Review). *Int J Mol Med*. 2015;35(1):10-16. https://doi.org/10.3892/ijmm.2014.1981.